Structure of aluminum, iron, and other heteroatoms in zeolites by X-ray absorption spectroscopy

Structure of aluminum, iron, and other heteroatoms in zeolites by X-ray absorption spectroscopy

by Jeroen A. van Bokhoven and Carlo Lamberti

was subsequently published in

Coordination Chemistry Reviews **2014**, *277–278*, 275–290

Published online 27 May 2014 on

http://www.sciencedirect.com/science/article/pii/S0010854514001489

http://dx.doi.org/10.1016/j.ccr.2014.05.013

Structure of aluminum, iron, and other heteroatoms in zeolites by X-ray absorption spectroscopy

Jeroen A. van Bokhoven [a,b*] and Carlo Lamberti [c,d*]

[a] *Institute for Chemical and Bioengineering, ETH Zürich, CH-8093 Zurich, Switzerland*

[b] *Swiss Light Source, Paul Scherrer Institute, CH-5232 Villigen PSI, Switzerland*

[c] *Department of Chemistry and NIS, CrisDi Interdepartmental Centers Center of Excellence, Universitàdi Torino and INSTM Reference center, University of Turin Center, Via P. Giuria 7, I-10125 Torino, Italy*

[d] *Southern Federal University, Zorge street 5, 344090 Rostov-on-Don, Russia*

* *j.a.vanbokhoven@chem.ethz.ch; carlo.lamberti@unito.it*

Abstract

Heteroatoms in zeolites provide them their catalytic activity. The silicon atom is always tetrahedrally coordinated and its valence IV, those of the heteroatoms much more varied. This is further complicated by the easy removal of heteroatoms out of the zeolite framework forming extra-framework phases. The change in coordination and removal of the framework atoms is often paralleled with enhanced catalytic performance and thus the precise characterization of heteroatoms in zeolites, as a function of synthesis and post-synthesis treatments, is topic of much research. In this review we summarize structural characterization of various heteroatoms using X-ray absorption spectroscopy. This method is in particular suitable, because it is element-specific, can be used to determine structure of amorphous samples, and can be applied under pretreatment and catalytic conditions. Aluminum shows a rich variation in coordination and, depending on the conditions, such as temperature and, notably, water content, zeolitic aluminum can be three, four, five and six-coordinate. The Brønsted acid site is associated with a strongly distorted tetrahedral coordination of the framework aluminum. During reaction, there is a large variation in extend of distortion and the flexibility of the zeolite framework to accommodate such structural differences is essential.

Iron in the zeolite framework is easily removed. The extra-framework iron species are extensively characterized, however, no consensus about their structure has been reached. Framework iron is Fe^{3+}, extra-framework iron mostly Fe^{2+}. The coordination of other tri- and tetravalent heteroatoms, such as gallium, boron, titanium, germanium, and tin are less investigated. It is however obvious that their structure is a function of the conditions the zeolite is exposed to. Like aluminum, the titanium atom easily switches coordination between four- and six-fold in a reversible way. All hetero-atoms often form extra-framework species. This review identifies the importance of changes in local structure of heteroatoms and the easy removal of these hetero-atoms from the framework. Often it is the extra-framework species that is responsible for catalytic activity.

Table of contents

Keywords: XAS; EXAFS, XANES; aluminum coordination; zeolite; heteroatom; iron speciation; in situ; operando

Highlights:

- The structure (oxidation state and or coordination) of hetero-atoms in zeolites is a strong function of condition
- Extra-framework species readily form
- XAS is excellently suitable for in situ and operando structural characterization of hetero-atoms in zeolites

1. *Introduction*

Zeolites are microporous crystalline silica frameworks that may incorporate hetero-atoms, of which aluminum is the most common [1-10]. Other often encountered examples are iron, titanium, gallium, germanium, boron, vanadium and tin [11-19]. Framework silicon atoms are tetrahedrally coordinated with oxygen atoms and occupy the so-called T-site (Figure 1) and each oxygen atom bridges two adjacent T-atoms. In the as synthesized materials, heteroatoms occupy these T-sites, substituting silicon. However, depending on the heteroatom valence state, on the presence/absence of charge balancing cations and on their nature (template cation, alkali-metal cation, NH_4^+, H^+ Brønsted site, etc…) the local environment of the heteroatom at framework position will exhibit different symmetry such as T_d, distorted-T_d and C_{3v}, see Scheme 1. Moreover, depending on the heteroatom nature and on the zeolite framework structure, heteroatoms have different stability and the simple template burning process or more severe post-synthesis treatments may cause the migration of a fraction of heteroatoms from framework into extra-framework positions. Consequently, the local structure, the accessibility, the reactivity and the nuclearity of heteroatoms may significantly deviates from the initially synthesized ones. The hetero-atoms location in zeolitic frameworks defines their unique catalytic behavior. Aluminum is responsible for Brønsted activity [20-24], titanium for (selective) oxidation reactions [17, 25] while iron and gallium are responsible for both activities, depending whether they occupy framework or extra-framework positions [26]. The presence of gallium makes zeolites active for aromatization reactions.

Because of the different charge between silicon (4+) and aluminum (3+), each aluminum atom in the framework requires cationic charge-balancing. Cations in the pores and cages supply this charge; these are called extra-framework species. If charge is balanced by protons the zeolite becomes Brønsted acidic [27-31] and a bridging hydroxyl group gives zeolites their catalytic activity [32-35]. Besides the cation exchange capacity, one of the most important features of zeolites is the presence of pores and cages in the size range between about half and one and a half nm [1, 4], giving them surface areas between about 100 to 500 m^2/g. Because of their intrinsic acidity, their stability, and large surface area, zeolites find widespread application in the oil refinery industry as catalysts and catalyst supports [31, 34, 36-47] and for molecular capture and separation [48, 49]. One of the largest catalytic processes is the FCC (fluid catalytic cracking) process [39, 44-46], which employs a modified zeolite (vide infra). In FCC, the high-boiling, high-molecular weight fraction of oil is cracked into smaller hydrocarbons, yielding more valuable products such as gasoline and olefins [50] The large surface area is appealing for its use as catalyst support.

The addition of a redox active element, such as iron, either in the framework replacing silicon atoms by synthesis or as extra-framework species by post synthesis modification, makes zeolites active in many oxidation reactions [26, 51]. Iron is an often used and studied element because iron-containing zeolites are active in the hydroxylation of benzene to phenol with nitrous oxide [52, 53], in the selective reduction of nitric oxide with ammonia [54] or hydrocarbons [54, 55], and in N_2O decomposition. [56-61].

Because zeolites are crystalline, structural characterization is seemingly straightforward and their crystalline structures are well known and documented by standard X-ray, neutron and electron diffraction methods [4, 11, 62-77]. Optimization of zeolites for catalytic applications involves structure modification for example by steaming [78-81], leaching [82-85] and introducing extra-framework species [26]. The result is the

occurrence of defects and amorphous species and secondary pore structures [82, 86-88]. The FCC catalyst for example is a steamed zeolite Y [39, 44-46], which contains mesopores and a significant fraction of extra-framework aluminum in the form of alumina and / or silica-alumina species [89]. In some FCC catalysts, the Brønsted sites may be partially replaced by rare earth metals such as cerium and lanthanum to provide improve the catalyst at both activity and stability level [90-93]. These structural changes are not captured by diffraction methods and characterization tools that do not rely on long range order must be applied to capture the defects and amorphous structures. The most-applied are ^{1}H, ^{27}Al, and ^{29}Si magic-angle spinning NMR [94-102] and infrared spectroscopy [23, 24, 100, 103, 104]. Two complementary, but much less frequently-used methods are X-ray photoemission (XPS) [101, 105, 106] and X-ray absorption spectroscopy (XAS) [107-109]. The latter has provided a wealth of structural data and insight into the zeolite structure and that of extra framework species, especially under non-standard conditions, as they occur during reaction and pre-treatment [107]. This manuscript deals with the application of XAS to determine zeolite structure. This synchrotron-based method probes electronic transitions, and thus probe density of states in a spin-selective manner [107, 109]. For example, at the Al K-edge a 1s electron is excited into the 3p density of states. Thus, non-bonding and anti-bonding states are probed and as these are sensitive to coordination and bonding, XAS probes the local structure. A decisive advantage of XAS is that it is element-specific, probes structure of matter irrespective of aggregation state [110-113], and can be applied under in situ conditions as routinely done in case of transition metals in zeolites [107]. It is a quantitative method; “no atom escapes detection”. This point is very relevant and discriminates XAS spectroscopies performed in transmission mode from other techniques such as e.g. EPR spectroscopy that probes only paramagnetic species or diffraction techniques that probes only the fraction of material characterized by long range order. As discussed in the following, the ability of probe all atoms of a specific element may also be a disadvantage of the method. This is the case of samples characterized by a high heterogeneity of species [107], that are characterized by complex XAS signals resulting from the average contribution from the different species. The disentanglement of the different contribution is not straightforward and requires independent information from other techniques and possibly the knowledge of the XAS spectra of the different species [114-118]. Differently from transmission mode, when fluorescence or electron yields modes are adopted [108, 109] then the XAS become surface selective and only atoms located between the surface and the convolution between penetration and escaping depths of the incoming and outcoming beams will be probed.

The Al K-edge, probing the 1s to 3p transition is at 1560 eV, which in the soft X-ray regime. Relatively few beam lines exist which enable measuring in this energy range, which may explain why there are not so many studies. An additional difficulty is the strong absorption of matter of X-ray radiation of such energy, which complicates measuring under conditions different from vacuum. As will be shown below, special cells and equipment have been developed [107], which enables measuring under conditions relevant to catalysis and pretreatment. This paper discusses the use of XAS to probe the structure of zeolites, that of extra framework species and their relation to catalysis. The first section deals with aluminum, because it is associated with catalytic activity of the zeolite framework and the modification of structure upon treatment is associated with change in catalytic performance. A brief introduction in the physical origin of the spectral

features in Al K-edge spectra and how these can be used to identify the different aluminum coordination in different samples and the changes in coordination that occur under different conditions, such as catalyst activation and true reaction conditions. Successively, XAS spectroscopy applied to investigate the structural and electronic configuration of the most relevant elements used as heteroatoms for isomorphous replacement in the zeolitic frameworks [11-16] is more briefly discussed in the following sections. The edges that are relevant to the manuscript are B, Ge, Ga, Fe, V, and Ti.
In this review we will focus on the characterization by X-ray absorption technique applied to the study of heteroatoms insertion in zeolitic frameworks; although relevant, the class of materials obtained introducing heteroatoms in aluminophospahate (AlPOs) and silicoaluminophosphate (SAPOs) frameworks [18, 64, 119-127] will be only barely mentioned. We just mention here that also for AlPOs and SAPO materials X-ray absorption technique played a key role in understanding the structural and electronic properties of the isomorphous substitution of different heteroatoms [127-136].

2. Aluminum in Zeolites

2.1. Theory and spectral features of Al K-edge XANES spectra

Many papers describe Al K-edge spectra experimentally and / or theoretically. The 1s to 3p transition is probed, which makes measuring Al K-edge spectra a very sensitive tool to differentiate the aluminum coordination, even in case of mixed coordination as described in this section. In compounds in which the aluminum coordination is distorted from pure centro-symmetric, thus away from perfectly octahedral, hybridization between the aluminum p and d orbital occurs, which affects the eventual spectral shape, such as appearance of a pre edge and a split whiteline. The origin of different characteristics to the spectra as described below, such as pre-edge, edge position, and resonances at particular energies are pretty well understood [137-139].
Al K-edge XAS was first used to determine the aluminum coordination in samples of geological interest [140-148]. From these and other studies characteristic spectral features are deduced that can be used to fingerprint and infer the presence and amount of specific coordinations [149, 150]. In short, there is a characteristic edge shift of a few eV between spectra of tetrahedrally and octahedrally coordinated aluminum (Figure 2, Table 1). Spectra of five-coordinate aluminum have the average edge position. Spectra of octahedral aluminum have a characteristically small pre-edge. The whiteline of tetrahedrally coordinated spectra is narrow, however less intense than that in spectra of octahedal compounds. Spectra of crystalline compounds of octahedral aluminum show a split whiteline, indicative of the symmetry around the aluminum atom. In general, two resonances of varying relative intensity are separated by about 4 eV. Spectra of tetrahedral aluminum have a broad band at about 20 eV above the absorption edge, the origin of which is mainly multiple scattering between aluminum and two oxygen atoms in the first coordination shell. In all cases, the first few features above and including the whiteline originate from multiple scattering over a long range. These features are therefore always more pronounced and defined in spectra of crystalline materials and have been used to detect aluminum-containing species of amorphous nature [151].
The aluminum 3p density of states is strongly affected by the hybridization with the 3s and 3d densities of states. Hybridization depends on symmetry: no p – d hybridization occurs in pure octahedral coordination; maximum hybridization in tetrahedral coordination. Perfect octahedral coordination yields spectra with a sharp whiteline; in case of the distortion from centro-symmetry splitting of the whiteline and appearance of

the pre-edge occurs because of the hybridization with the d density of states (vide infra). As said, the XAS near-edge spectra contain small resonances at different energy position, which originate from multiple scattering over an extended range. Thus, the near-edge region is theoretically only reproduced assuming large clusters and contains information about the long-range zeolite order. More recently, the influence of atomic vibrations on Al K-edge X-ray absorption near edge structure (XANES) are predicted to enable electric-dipole transitions to 3s and 3d final states. The result is the occurrence of sizeable transitions to 3s final states, leading to improvement of theory and experiment [152]. In general, spectra can be theoretically simulated to great agreement with experimental ones [153].

The theoretical understanding of the origin of spectral resonances and the excellent agreement between theory and experiment yield confidence to structure determination from experimental XANES spectra that are not represented in existing databases, making it a first-rate tool to follow aluminum coordination under non-standard conditions as they occur during catalysis and sample treatment.

2.2. The local aluminum coordination and the Brønsted active site

One of the first systematic X-ray absorption studies at the Al K-edge on zeolites was performed by Froba et al. [154]. They measured zeolite sodalite that had different exchanged ions $[Na_4X][Al_3Si_3O_{12}]_2$, with $X=Cl^-$, NO_2^-, $B(OH)_4^-$, respectively $½CrO_4^{2-}$ in the zeolite pores. The size of the anion affects the Al K-edge spectra to a large extent. While the Al-O and Si-O bond lengths are insensitive to the extra-framework species, the Al-O-Si bridging angle affects the Al K-edge absorption spectra. The distance between Al and Si atoms and the presence extra-framework ions in the zeolite pores influence the multiple scattering and thus the resonances in the energy range between about 5 and 20 eV above the absorption edge. These features are thus reminiscent of the long range order about tetrahedrally coordinated aluminum in zeolites.

Koningsberger and Miller [155] were the first to determine the local aluminum structure associated with the zeolitic Brønsted acid site by full EXAFS analysis at the Al K-edge. A major outcome was that even within the short data range that is accessible at the Al K-edge, because of the closeness of the Si K-edge, structural information about the aluminum could be achieved. The Al K-edge is at 1560 eV, that of silicon 1839 eV, resulting in a useful k_{max} of about 8 $Å^{-1}$ at the Al K-edge. This limits the r-space resolution that can be achieved to about 0.15 Å and the number of independent parameters that is accessible (between 5 and 7 for the first shell analysis) [107]. A clear difference in local structure around the framework aluminum atom was observed for charge-balancing cations H^+, Na^+, and NH_4^+, see Scheme 1a. The longest average Al-O bond length of 1.700 Å was observed in H-Y zeolite. The four Al-O bond lengths in Na-Y and NH_4-Y are 1.636 respectively 1.620 Å. This analysis laid the basis for further and more detailed studies on the local structure of framework aluminum. Later, van Bokhoven et al. [156] (vide infra) and Joyner et al. [157] determined the local aluminum coordination associated to the active site. The local structure in zeolites H-MFI, H-Y, and Na-Y zeolites was determined (Table 2). It was convincingly shown that asymmetry in the tetrahedrally coordinated framework aluminum exists when protons are charge balancing. One long aluminum – oxygen bond accompanies three shorter ones (Scheme 1a, right side). The long Al-O bond correlates to the oxygen atom that binds the proton. The long Al-O bond is somewhat shorter in zeolite H-Y than in H-MFI (1.87 vs 1.98 Å). Around the same time, theoretical studies by the groups of Sauer and van Santen were

conducted that had predicted the strong asymmetry in the tetrahedral aluminum coordination in case of proton-exchanged zeolites, which was now convincingly experimentally confirmed [158, 159]. Interestingly, when these studies were performed, the aluminum associated with the Brønsted acid site was sometimes considered to be invisible in ^{27}Al MAS NMR [160]. Measuring ^{27}Al MAS NMR on zeolites in dehydrated conditions leads to significant spectral broadening because of the quadrupolar nature of the aluminum nucleus.

The capability of XAS to measure catalyst structure under in situ conditions has been exploited. An in situ cell, called ILEXAFS (in situ low energy X-ray absorption fine structure) [161, 162], was specifically designed and constructed for this purpose. A temperature range from liquid nitrogen up to 700 °C could be achieved at a gas pressure of maximally one bar (Figure 3). Later, simpler designs, based on transmission mode measurements were constructed and also used for measuring the aluminum coordination in zeolites [163, 164]. Within ILEXAFS, the local structure of framework tetrahedrally coordinated aluminum was followed during a catalytic reaction. The change in the local aluminum coordination is schematically shown in Figure 4, which is based on the experimentally determined values in Table 3. NH_4-Y zeolite, with its 12 membered ring pore opening and large super cages, was treated in situ at high temperature forming the catalytically active Brønsted acid site in H-Y zeolite. In accord with the later reported data of Joyner et al. [157], the symmetric coordination of aluminum in NH_4-Y becomes distorted upon removing NH_3 and formation of H-Y. Admission of ethylene at room temperature causes reaction of the olefin and adsorption of a reacted species onto the acid site, decreasing the longest Al-O bond length from 1.89 to 1.81 Å (Table 3). This is in agreement with various studies that showed that upon adsorption of a base on the zeolite acid site, the distortion of the tetrahedrally coordinated aluminum decreases [165-167]. The oligomerization forms larger hydrocarbon species, possibly carbenium ions, that may form alkoxides on the conjugated base, as is indicated by a change of color of the sample from white to grayish black. Increasing the temperature restored the long Al-O bond, which indicates that the reacted intermediate no longer interacts with the acid site. Coking of the zeolite after desorption of the alkoxide reinstates the acid site and thus the asymmetric aluminum coordination. To date, this study remains the only one based on Al XAS that report data under catalytic conditions.

Drake et al. also measured the local aluminum structure as function of the charge-balancing cation by Al K-edge EXAFS. The results were largely in accord to those above and confirmed again the strong distortion of the framework tetrahedrally coordinated aluminum by lengthening of the Al-O(H) bond [163]. Overall, these studies indicate that the framework of a zeolite shows large flexibility in accommodating extra-framework cations and reactive intermediates. Changes in the local structure of the active site occur already under relatively mild conditions. Proton-exchanged zeolites show a particular strong distortion of the local aluminum coordination. Al K-edge EXAFS is a sensitive tool to determine the structure of the catalytically active site, which is surprisingly little exploited.

2.3. Effect of extra-framework cation and temperature on aluminum coordination

Zeolite beta was the first clear example of a zeolite which shows a reversible change in aluminum coordination [168]. When the charge-balancing cation is sodium or potassium, all aluminum atoms have a tetrahedral coordination; when exchanged to NH_4^+ and after

NH_3 removal, a large fraction of aluminum (up to about 25%) changes coordination to octahedral. Adsorption of a strong base, such as pyridine and ammonia allows for all the aluminum atoms to recover the tetrahedral symmetry. Later, it was shown that this is a general property of zeolites [169, 170] and silica aluminas [171]. A large influence of the Si/Al ratio on the formation of octahedrally coordinated aluminum was observed, the higher the ratio, the lower the amount of octahedrally coordinated aluminum [172]. The ability to measure aluminum coordination under in situ conditions was exploited by various research groups, employing the previously shown ability to determine aluminum coordination relatively easily from XANES analysis (Table 1 and Figure 2).

Commercially used zeolites are often steamed, which leads to the presence of extra-framework species, which are generally assumed to help stabilize the framework. Moreover, such species are often assumed to enhance the reactivity of the framework Brønsted acid sites. Al K-edge XANES and EXAFS has identified that the aluminum coordination in steamed zeolites is a function of temperature and notably the water content. Exposure of an acidic zeolite to water leads to the formation of octahedrally coordinated aluminum, its amount depending on Si/Al ratio and zeolite structure [172]. In situ XANES at the Al K-edge on acidic zeolites identified a variation in coordination with temperature and the presence respectively absence of water. For example, a steamed zeolite Y, also called USY contains a large fraction of extra-framework aluminum under hydrated conditions. Heating such sample results in the loss of octahedral aluminum and appearance of tetrahedrally coordinated aluminum [163]. An identical behavior was observed in amorphous silica alumina (ASA), thus confirming that extra framework ASA forms during steaming [170]. Below, it will be shown that the octahedrally coordinated aluminum in acidic zeolites may form at room temperature after exposure of the sample to moisture.

The conditions of catalytic reactions, notably, the presence of bases, reaction intermediates, and water and the temperature thus affect the local structure of the active site in zeolites. Especially, at high Si/Al ratio and thus low aluminum content, crystallography fails to capture the local structure around the aluminum [106].

2.4. High temperature zeolite structures, the presence of three-coordinate aluminum

Compared to Brønsted acidity, Lewis acidity in zeolites is poorly understood. It is associated with under-coordinated aluminum. In the previous section, it was shown that water yields a large fraction of octahedrally coordinated aluminum in proton-exchanged zeolites, which may be seen as adsorption of Lewis base water on a Lewis acid. Thus, in these cases, tetrahedrally coordinated aluminum functions as the Lewis acid. However, the occurrence of three-coordinate aluminum has been often invoked to be responsible for Lewis acidity. Because the Al K-edge probes the empty p density of states on the aluminum, spectra of three-coordinate aluminum are expected to show a pronounced pre-edge, which is confirmed by FEFF simulations that calculate the presence of a pre-edge feature upon breaking of one of the aluminum – oxygen bonds of the tetrahedrally coordinated framework aluminum [173]. Al K-edge XANES was measured at temperatures in access of 400°C under vacuum. At such high temperature, a pre-edge feature appeared in the spectra; its intensity increased with temperature. The feature was observed in proton-exchanged zeolites mordenite and beta, the latter, steamed and unsteamed. Because of the temperature, there is a very large disorder, which could have been responsible for the pre-edge [152]. However, cooling to room temperature caused

only a minor change in the spectral shape, excluding a major effect of temperature on the spectra. Based on the FEFF simulation, it was concluded that the high temperature induces a coordination change, forming an estimated fraction of about 5 to 10% three-coordinate aluminum [174]. Addition of even traces of water at room temperature, causes the rapid disappearance of the spectral pre-edge feature of three-coordinate aluminum, which was accompanied by formation of spectral intensity right above the absorption edge, indicative of formation of octahedrally coordinated aluminum. A logical conclusion is that three-coordinate aluminum is associated with a defect site that adsorbs water, forming six-coordinate aluminum. This process may be accompanied by further structural collapse. Later studies showed that even in the presence of water in access of about 450 °C, three-coordinate aluminum forms without evidence of octahedrally or five-coordinate aluminum formation. Such species only form at lower temperature, when the pores fill with an access of water [164, 175].

3. Isomorphous substitution of Fe^{3+} in zeolitic frameworks

The role of Fe K-edge XAS in the investigation of the both the structural and electronic properties of iron atoms in zeolites has been very relevant [176-198]. NMR, which has been so relevant for investigating aluminum species in zeolites (see Section 2), is hampered in Fe-zeolites by the low natural abundance of ^{57}Fe, by its very low gyromagnetic ratio, and by the paramagnetic nature of most of the iron complexes. Other relevant techniques are Mössbauer [183, 199-204], FTIR [26, 205-210], UV-Vis [26, 195, 211], EPR [206, 211, 212] and Raman [213] spectroscopies.

3.1. Catalytic relevance of Fe-zeolites

Iron containing zeolites in general [16], and Fe-MFI in particular [63], are deeply investigated as they show high activity in the hydroxylation of benzene to phenol with nitrous oxide [52, 53], in the selective reduction of nitric oxide with ammonia [54] or hydrocarbons [54, 55], and in N_2O decomposition [56-61]. The active species in Fe-zeolites are extra-framework iron species that originate from lattice sites upon thermal activation [190, 195, 205-209, 212-220] or that are introduced into the zeolite channels via post-synthesis methods [180, 181, 199, 209, 221-224].

3.2. XANES characterization of Fe-zeolites

As was the case for aluminum, Fe XANES studies on minerals [225-235] and theoretical studies [236-239] have been of great relevance to determine the most relevant fingerprints of the Fe K-edge XANES spectra. As a typical example, Figure 5 reports the effect of template burning in air and successive activation in vacuo at increasing temperature on the XANES features of a Fe-MFI sample. The most evident variation is the red-shift of the edge position, which moves from 7123.6 eV for the sample measured with template (blue line) to 7122.4 and 7120.6 eV for the samples activated at 773 K (orange line) and 973 K (red line) respectively. An even larger shift was observed when the activation was done at 1073 K (gray curve). These data provide clear evidence that iron in the as-prepared sample is present as Fe^{3+}. The thermal activation causes Fe^{3+} species to undergo reduction to Fe^{2+}.

Besides the changes in the edge and the near-edge region, also the pre-edge features are affected by the thermal treatment. The spectrum of the as-prepared sample is characterized by a strong and sharp $1s \rightarrow 3pd$ pre-edge peak around 7114.2 eV (as emphasized in the inset), whose intensity is even higher than that of $FePO_4$ model compound (0.205 *vs.* 0.133, being the edge jump normalized to unit), indicating that the

local symmetry of Fe^{3+} in the MFI framework is closer to the ideal T_d than iron in $FePO_4$ [190, 206]. This is due to the template, and the iron atom has four equivalent Fe-O bonds at 1.86 Å, while for ferric phosphate two distinct pairs of Fe-O bonds at 1.82 and at 1.87 Å are present [240]. Successive thermal treatment causes a simultaneous decrease of the $1s \rightarrow 3pd$ peak intensity and a low energy shoulder increase in the $1s \rightarrow 3pd$ resonance. The energy position of this new component (around 7111.8 eV) is close to that observed for the $FeCp_2$ (Cp = cyclopentadienyl i.e. $C_5H_5^{\cdot}$) model compound (7112.5 eV) [190, 206]. However, the higher full-width at half maximum indicates the presence of more than one Fe^{2+} species, in agreement with the high heterogeneity of extra-framework iron species present in zeolitic frameworks. In conclusion, XANES studies, summarized in Figure 5 demonstrate that in the in situ activated Fe-MFI sample, a significant fraction of iron migrated from the framework tetrahedral position into extra lattice Fe^{2+} species. A similar behavior has been observed by removing the template in the Fe-MCM-22 system [219, 220]. Different results were obtained by Joyner and Stockenhuber [182], who used XANES spectroscopy to investigate the oxidation state of iron in ion-exchanged Fe-ZSM-5 samples where only Fe^{3+} species have been detected. This fact underlines the importance of the preparation method in the iron speciation.

Finally, the white line (first resonance after the edge) of the XANES spectra reported in Figure 5 is very informative, because its intensity reflects the coordination of the absorbing atom. The sample with template shows a white line intensity similar to that of $FePO_4$ (1.31 *vs.* 1.35, being the edge jump normalized to unit), much lower than that observed for six-fold coordinated model compounds (between 1.52 and 1.60), reflecting the four-fold coordination of iron in the as-prepared sample [190, 206]. Migration of Fe^{3+} to extra-framework positions causes a progressive decrease of the white line intensity: from 1.23 to 1.20 for sample activated at 773 and 973 K respectively (Figure 5). This further decrease of the white line intensity argues, for the samples investigated by Berlier et al. [190, 206], against the presence of a considerable fraction of iron species in aggregated clusters, suggesting the presence of isolated iron species exhibiting a high coordinative unsaturation. This picture has been strongly supported by infrared data of adsorbed NO published in different contributions [190, 205-209].

3.3. EXAFS characterization of Fe-zeolites

As already discussed for the Al local environment in zeolites (Section 2.2 and Scheme 1a), the local environment of the trivalent Fe^{3+} heteroatom hosted in the MFI framework is tetrahedral, exhibiting 4 equivalent Fe–O bonds at 1.85 Å in presence of the tetrapropyl ammonium hydroxide ($TPAOH^+$) template, that moves to 1.86 Å when the counter ion is NH^{4+}. Bordiga et al showed that [195], when the counter ion is the proton (Brønsted site), then the tetrahedral symmetry of Fe^{3+} is strongly distorted, showing a long Fe–O bond at 2.10 Å, due to Fe–(OH)–Si bridge and the shorter ones at 1.865 Å due to three equivalent Fe–(OH)–Si bridges, see also Table 4.

Different catalytic mechanisms have been hypothesized so far to explain catalytic activity of Fe-zeolites. However, there is no general consensus on the nature of the active iron site: isolated [187, 205-207, 219, 220], di-nuclear [56, 180, 181, 222-224, 241] and poly-nuclear [242] Fe species have been put forward. The situation is complicated, because the relative fraction of the three species in a given sample strongly depends on the preparation procedure, the iron content, and the post synthesis treatments.

The determination of the nuclearity of the extra-framework iron species in Fe-zeolites is obviously of fundamental relevance. Due to both its atomic selectivity and its local nature, EXAFS is in principle the technique of choice to discriminate among isolated, dimeric and polymeric Fe species. However, severe reproducibility problems are present when looking to results coming from different laboratories. On a simple statistical ground, it is evident that di-nuclear and aggregated iron species are more abundant at high iron loading, especially when post-synthesis methods are used. Conversely, aluminum-containing Fe-ZSM-5 samples with low iron loading, and highly active in selective oxidation reactions [52, 53, 243], show mainly isolated extra-framework Fe^{2+} species, mostly located in the vicinity of framework aluminum species [187, 188, 207, 244-246].

A careful look into the literature yields no unified model to define the local structure of iron species hosted in zeolites. Figure 6 summarizes the different Fe-O, Fe-Fe and Fe-Si/Al distances reported in the literature from EXAFS data and here plotted as a function of iron content (ordinate axis) [176-196].

The results are heavily scattered: in particular, at low iron concentration (from 0.2 to 1.0 wt %), the Fe-O distances are found in the 1.78 - 2.40 Å range, a spread much higher than the typical accuracy of bond length distance detected by EXAFS ($\pm$ 0.01 or $\pm$ 0.02 Å). Concerning other distances measured in EXAFS experiments, most of the Fe-Fe distances in iron containing MFI appear centered close to the values expected in α-Fe_2O_3 (see the two vertical dashed lines in Figure 6). It is well known that clustered iron species contribute to the FT of the EXAFS function with signals between 2 and 4 Å in the FT. By fitting the EXAFS contribution in the 2-4 Å interval with a Fe-Fe model once could in principle obtain the average Fe-Fe coordination number ($N_{Fe\text{-}Fe}$) [183, 185, 189]. Unfortunately, the relationship between such $N_{Fe\text{-}Fe}$ value and the average Fe nuclearity is far from straightforward, because complexity is introduced by the heterogeneity of extra-framework species [190]. As a consequence, an average Fe-Fe coordination number of e.g. $N_{Fe\text{-}Fe}$ = 1.0 could be interpreted as 100% of dimers, as 50% of isolated monomers and 50% of trimers (having two iron neighbors) or as 67 % of isolated monomers and 33 % of tetramers, and so on. The situation is even more complex, because the 2-4 Å interval is the region where also the backscattering of the framework T-atoms aluminum and silicon is. Consequently, the Fe-Fe distances are superimposed to those of Fe-Si/Al in the 2.80 to 3.20 Å range. The scattering of both Fe-O and Fe-Fe distances can be explained by two main reasons. (i) The Fe-zeolites investigated by different groups might be significantly different, since the final form of iron species is strongly affected by the preparation procedure. (ii) Notwithstanding the fact that the accuracy of a first shell distance determination is in principle as good as $\pm$ 0.01 or $\pm$ 0.02 Å, these error bars are statistical and systematic errors are not accounted for. In the specific case of Fe-zeolites systematic errors may have a double origin. Usually phase-shifts and amplitude functions, which are crucial in determining bond distances and coordination numbers, are theoretically generated from a guessed cluster. As the actual geometry of the active iron species is a priori unknown, phases and amplitudes generated in that way can be questionable. The second source of possible systematic errors is the assumption of a Gaussian distribution of distances which is done in the standard EXAFS formula, usually used in most of the cited papers. It is well known that in systems characterized by a high degree of heterogeneity, like liquids or amorphous systems, this assumption is no longer valid. In such cases, EXAFS data should be analyzed according to the cumulant approach [107, 247-249].

The results summarized in Figure 6 deserve some additional comments. In particular, the Fe-O distance at about 1.4 Å found by Choi *et al.* on oxidized samples could be consistent with the formation of Fe(IV)=O species [187, 188]. Moreover, some of the distances centered at about 2.5 Å, ascribed to Fe-Fe scattering and used to argue for the presence of di-iron-oxo species, may be due to Fe-Cl groups on samples prepared from $FeCl_3$ exchanged systems. In this regard, the group of Bell [187] gave a different explanation. They showed that the peak at 2.5 Å, was not due to Fe-Fe contributions, but was actually due to Fe-Al contributions. They were able to support this thesis by arguing that (i) the imaginary part of the peak has the same characteristics as that generated theoretically for Fe-Al backscattering, whereas it differs distinctly from that generated theoretically for Fe-Fe backscattering; and (ii) the structure of the peak, measured for different samples, does not change significantly with Fe/Al ratio and was unaffected by sample treatment. They concluded that the iron in Fe-ZSM-5 is present as isolated cations associated with framework aluminum [187]. In this regard, two contributions from the group of Grünert [185, 189] are worth of note. In the first work [185], the authors found a significant discrepancy between iron nuclearity derived from EXAFS, TPR, and Mössbauer spectroscopies. Analogously, in their last work [189] an apparent discrepancy between the results of UV-Vis and the EXAFS analysis has been evidenced. The former work indicated the almost exclusive presence of isolated iron sites, whereas the latter work suggested clusters of a few iron atoms. The high $N_{Fe\text{-}Fe}$ suggested from EXAFS may be due to the fact that backscattering by framework silicon or aluminum atoms was attributed to iron. The important message coming from the works of Grünert et al. [185, 189] is that the use of other independent characterization techniques is important to minimize the risk of misinterpretation of the EXAFS results.

4. Insertion of other trivalent elements in zeolitic frameworks

4.1. Ga-zeolites

The interest in gallium-containing MFI-type zeolites stems from their and from their selectivity in the propane aromatization [250] and in general for their high selectivity to aromatics in the catalytic conversion of olefins and paraffins following the so-called Cyclar process [251-253], from their high catalytic activity for vapour-phase conversion of phenol and ammonia mixtures into aniline [254] n. There is evidence that enhanced aromatization on gallium-containing zeolites is the result of a bifunctional catalytic process involving both framework and extra-framework gallium atoms [255-258].

For these materials, the most used characterization techniques are IR [259], ^{71}Ga MAS NMR [260], and XAS [218, 261-270] spectroscopies. Both Ga K-edge XANES and EXAFS spectra have been important to determine the Ga coordination, local symmetry and to differentiate between framework and extra-framework species. XAS has been applied to both samples where gallium has been introduced during the synthesis [218, 261-266] and after post-synthesis treatments [267-269]. Of interest is also the XAS study of Okumura et al. [270] on Ga-MCM-41.

Scheme 1a, already discussed for the Al^{3+} and Fe^{3+} (see Sections 2.2 and 3.3, respectively), holds also for the local environment of the trivalent Ga^{3+} heteroatom hosted in the MFI and BEA frameworks. This has been proven by in the Ge K-edge EXAFS study by the group of Lobo [266], who found 4 equivalent Ge–O bonds in $TPEOH^+$-Ga-β, NH_4^+-Ga-β, $TPAOH^+$-Ga-ZSM-5 and NH_4^+-Ga-ZSM-5 zeolites, while in H^+-Ga-β (H^+-Ga-ZSM-5) zeolite they found a stretched Ga–(OH)–Si bond at 1.99 Å (2.02 Å) and three shorter Ga–O–Si bond at 1.79 Å (1.80 Å), see also Table 4 .

The modification of the local environment during the template removal and successive thermal treatments allowed to observe the progressive migration from isolated tetrahedral framework sites into aggregated extra-framework positions [218, 263-266] similar to what was already discussed in the case of iron isomorphous substitution, vide supra Section 3.
Of particular interest is the XAS study of Walton and O'Hare [271] who investigated at both the Ga and Si K-edges the amorphous gallium silicates isolated in the early stages of the hydrothermal synthesis of the gallium silicate zeolite hydroxosodalite. The local structure of the amorphous phases is found to resemble the structure of the zeolite. The authors observed the evolution from the six-fold coordinate gallium atoms in the amorphous starting material to the four-coordinate environment similar to that found in the final crystalline Ga-zeolite material. Both gallium and silicon environments exhibit some degree of medium-range order in the amorphous materials. This is indicative of an extended network constructed from alternating $Ga(OSi)_4$ and $Si(OGa)_4$ units forming the structure of the amorphous materials, reminiscent of the structure of the zeolite [271].

4.2. B-zeolites

In this short paragraph we summarize the works of Regli et al. who investigated by means of FTIR [272], B-K-edge XANES and DFT calculations [273, 274] the isomorphous substitution of B^{3+} into the CHA framework (B-SSZ-13) before and after template removal, and after interaction with NH_3.
B K-edge XANES spectra of B-SSZ-13 in the presence of template (red curve), after calcination (blue curve) are reported in Figure 7a. The as prepared B-SSZ-13 exhibits $[B(OSi)_4]$ units in T_d-like geometry (sp^3-hybridized B atoms) while, upon template burning, the break of a B-O-Si bond results in $[B(OSi)_3]$ units in D_{3h}-like geometry (sp^2-hybridized B atoms) [273, 274]. The XANES study fully confirms the parallel infrared experiment (Figure 7b) [272], where template removal results in the appearance of the strong IR band at 1390 cm^{-1}, due to the asymmetric B-O stretching [275-277]. This reaction scheme is depicted in the evolution form the red to the orange inset in Figure 7.
Indeed, the spectrum collected in presence of template is characterized by three main components at 194.4, 198.5 and 203.0 eV, whose intensities are 1.0, 1.4 and 1.3, respectively. The components at 198.5 and 203.0 eV were assigned to B in sp^3 hybridization on the basis of comparison with the spectra observed in the BO_4 tetrahedral units of bulk BPO_4 [278], in bulk cubic BN [279], and in amorphous B-P-silicate [280], where the presence of phosphorus forces boron atoms into tetrahedral coordination. In B-SSZ-13 the relatively broad nature of these bands was attributed by Regli et al. [274] to a distortion of BO_4 tetrahedra that results in the loss of the degeneracy of $\sigma^*(t_2)$ orbitals and the consequent broadening of the transitions. In particular, the component at 198.5 eV was assigned to transition from B(1*s*) state to anti-bonding (σ^*) states (T_2 and A_1 symmetry) of tetrahedral BO_4 groups. Finally, the feature at 194.4 eV, was attributed to the B $1s \rightarrow \pi^*$ resonance, which is associated with sp^2 hybridization and planar bonding [279-281]. It is worth noticed that, in the B-SSZ-13 sample with template, the fraction of B atoms that exhibit a planar geometry with sp^2 hybridization is very low, as the $1s \rightarrow \pi^*$ resonance gives rise to very sharp and intense peaks in materials exhibiting only this phase. In the XANES spectrum collected on the calcined B-SSZ-13 sample (blue curve in Figure 7) both features at 198.5 and 203.0 eV, ascribed to B in sp^3 hybridization, disappear and where the 194.4 eV component dominates the spectrum, having an intensity as high as 8.2 and a FWHM as narrow as

0.55 eV. Actually, this component is the fingerprint band of B species having sp^2 hybridization [279].
As a conclusion, the works of Regli et al. [272-274] showed how B^{3+} is not following the general behavior of the other trivalent heteroatoms discussed above, see Sections 2.2, 3.3 and 4.1. In this case, the Scheme 1a does not hold and should be remplaced by the scheme reported in the inset of Figure 7a.

4.3. Cr- and Mn-zeolites
Chromium(III) has been much less used as heteroatom in zeolites and only few papers refer to the material synthesis and characterization by IR, EPR UV-Vis, XRPD and ^{53}Cr solid state NMR [282, 283]. In particular, the IR band at 960 cm^{-1}, similar to that found in Ti-silicalite-1 (vide infra Section 5.1), testified the isomorphous insertion in the zeolitic framework. To the best of our knowledge, no Cr K-edge study has been carried out so far on such materials. Conversely, the literature is more abundant for the isomorphous insertion of Cr^{3+} inside aluminophospahate frameworks (AlPOs) [135, 136] Also Manganese(III) was inserted in the MFI framework, the material was investigated by combined XRPD, IR, Mn K-edge XANES and EXAFS Mn-silicalite-1 [284]. The authors found first shell oxygen atoms at 1.93 Å.

5. Insertion of tetravalent elements in zeolitic frameworks
5.1. Ti-zeolites
The selective catalytic oxidation of organic compounds with an environmental attractive oxidant, aqueous H_2O_2, is a challenging goal of fine chemistry. Over the past two decades, heterogeneous titanium(IV)-based catalysts have received much attention for their application in this field [25, 285, 286]. Highly active and selective catalysts can be produced by dispersing titanium atomically in a silica matrix [287], or by grafting isolated titanium species to the surface of silica [288] mesoporous molecular sieves [289-292], layered aluminosilicates [293], polyoxometallates [294, 295] or by isomorphously substituting titanium (less than 2-3 wt.%) for silicon in molecular sieve frameworks [25, 296-301], that are relevant for this review. Titanium silicalite-1 (TS-1) belongs to this last category as it is obtained by inserting titanium into the MFI lattice [25, 296, 298-301]. The coordination and aggregation states of Ti(IV) in zeolitic framework has been investigated by means of diffraction techniques [302-305] (looking to the cell volume expansion), infrared and Raman [300, 306-317], UV-Vis [300, 308, 309, 312] while EPR was able to detect reduced Ti(III) species [318, 319]. Also in this case Ti K-edge XAS techniques played an important role [215, 218, 292, 300, 301, 308-312, 320-332]. Theoretical calculations [313-317, 325, 326, 333-343] coming from different groups supported the experimental findings obtained on well prepared materials.
As was the case for aluminum and iron, also for titanium, the investigation of minerals with titanium species having a defined oxidation state and occupying well defined crystallographic sites provided an important database of XANES spectra of model compounds [344-347].
The isomorphous substitution of Ti(IV) into silicon tetrahedral framework position is straightforwardly detected in vacuum activated zeolites by XANES technique. The spectra in the pre-edge region are characterized by a narrow and intense peak at 4967 eV, due to the $1s \rightarrow 3pd$ electronic transition involving Ti(IV) atoms in tetrahedral coordination [108, 215, 301, 308, 309, 311, 348-350], see black spectrum in Figure 8. The same electronic transition for Ti(IV) species in TiO_2 (anatase or rutile) [351, 352] or

in ETS-10 titanosilicate [109, 348, 353, 354], where Ti(IV) species are in octahedral environment, is characterized by a very low intensity due to the small *pd* hybridization which occurs in octahedral symmetry. Indeed, the transitions $A_{1g} \rightarrow T_{2g}$ are symmetrically forbidden in the case of octahedral coordination while the transition $A_1 \rightarrow T_2$ is allowed in the case of tetrahedral coordination, as in the case of [TiO_4] units hosted in the dehydrated MFI framework [215, 301, 308, 309, 348, 350]. This explains why the 4967 eV pre-edge peak, very intense for the activated Ti-zeolites, is strongly depressed in presence of adsorbates like H_2O or NH_3 [301, 310, 312, 320], see Figure 8 and Scheme 1b, or before calcination, as the template molecule enters the first coordination shell of Ti(IV) [218]. Of relevance is the reversibility of the H_2O, NH_3 and even H_2O_2 absorption: a mild activation in vacuo condition restores the T_d symmetry of Ti(IV) centers [301, 309, 310]. The typical average Ti-O distance in TS-1 is 1.79 ± 0.01 Å in vacuo (the T_d symmetry) that moves to 1.82 and 1.83 Å upon adsorption of H_2O and NH_3, respectively [301], see Scheme 1b. It is finally worth noticing that it was generally believed that Ti(IV) centers in TS-1 are able to coordinate 2 water (ammonia) molecules in their first coordination shell. Only very recently, using valence-to-core X-ray emission spectroscopy [355, 356] coupled with DFT calculations, Gallo et al. [341, 342] showed that only one water (ammonia) molecule is adsorbed on Ti(IV) centers.

5.2. Other tetravalent elements: Ge- and Sn-zeolites

Germanium(IV) has been successfully inserted in the MFI framework [11, 12, 357, 358]. Tuilier et al. [357] investigated the Ge-ZSM-5 system at two different germanium loading both before and after template removal, proving the isomorphous substitution of germanium in the framework. They found a contraction the Ge-O bond distance from 1.75 ± 0.02 Å to 1.72 ± 0.02 Å after template removal.

Tin(IV) has been introduced in the BEA framework by the Corma group [359, 360] and by Maki-Arvela et al. [361], that also prepared a Sn-Y sample. Of particular interest for this review is the work of the Corma group [359, 360] because authors treated the Sn K-edge EXAFS data with a multi-shell fit that showed how Sn does not randomly insert into the beta-zeolite structure but rather occupies the T5/T6 sites in the six-membered rings, being substituted in pairs on opposite sides of these six-membered rings. The authors claimed that this specific, uniform crystallographic location of the Sn in the BEA framework is the key in understanding the uniform catalytic activity and the high chemical selectivity demonstrated for this catalyst that behaves in an almost enzyme-like selectivity of this catalyst in Baeyer-Villiger oxidations. The approach used to analyze the EXAFS data is very original as this EXAFS study made an attempt to enter the domain of preferential isomorphous substitution of heteroatoms in zeolites, that is usually treated with diffraction techniques [86, 302, 303, 362-365] or with very complex synchrotron-based techniques such as X-ray standing waves [366]. To the best of our knowledge no successive work was able to use EXAFS data to discriminate a preferential insertion of a heteroatom among the different crystallographic T sites available in a zeolitic framework.

More recently, the insertion of Zr^{4+} in the MFI has been claimed [367, 368] based on XRPD, FTIR UV-vis and TG analyses. To the best of our knowledge, no Zr K-edge X-ray absorption study on such material has been carried out so far.

6. . Insertion in zeolitic frameworks of heteroatoms of less common valence state

6.1. Insertion of pentavalent elements in zeolitic frameworks

Arsenic(V) has been inserted in the MFI framework [369], but, among pentavalent elements, vanadium(V) is by far the most used for isomorphous insertions in zeolitic frameworks. Vanadium-substituted zeolites have been widely investigated by laboratory IR, Raman, UV-Vis, photoluminescence, ^{51}V solid state NMR and EPR spectroscopies [11, 18, 19, 370-375] and by synchrotron radiation based X-ray absorption spectroscopies [376-384]. The most investigated system was V-MFI, also called VS-1, in analogy with the notation of TS-1 for the insertion of titanium in the same framework. For the same reason the insertion of vanadium in the BEA framework has been called VS-2. Under UV irradiation, VS-1 and VS-2 exhibit an interesting photocatalytic reactivity for the isomerization of 2-butene and decomposition of NO into N_2 and O_2 at room temperature [376, 377, 385, 386].
The local environment of V^{5+} species inserted in zeolitic frameworks differs significantly to that of the trivalent and tetravalent elements discussed so far. The V K-edge EXAFS experiments of the Anpo group clearly showed that V^{5+} species are linked to the zeolitic framework through three V-O-Si bonds exhibiting an average V-O distance of 1.78 Å (1.73 Å) when hosted in the VS-1 (VS-2) framework and exhibit a fourth oxygen atom located at a much shorter distance (1.68 and 1.64 Å in VS-1 and VS-2, respectively) due to a V=O double bond [378, 383], see Table 4 and Scheme 1c. The local environment of V^{5+} such species is tetrahedral-like in C_{3v} symmetry, as confirmed by a sharp and intense pre-edge peak in the V K-edge XANES spectra [378, 383].

6.2. Insertion of divalent elements in zeolitic frameworks

The insertion of divalent heteroatoms in zeolites is much less common than the case of tri- tetra- and pentavalent elements. This is because the difference of two formal charge units with respect to the silicon of the SiO_4 units makes the isomorphous substitution with Si(IV) not straightforward. For this reason the literature is much wider for the insertion of divalent heteroatoms in AlPOs and SAPOs frameworks [121, 125, 127-131, 134], where isomorphous substitution in P(III) sites implies a difference in the formal charge of one unit only. Notwithstanding such difficulties few reports are present in the literature [136, 283, 387-392] and among them we stress the work of Lita et al. [392] who reported the insertion of Mn^{2+} in the silicalite-2 (ZSM-11 or MEL) framework. The isomorphous substitution into Si^{4+} sites has been proved by EPR, and Mn L_{III} and L_{II}-edges. The authors found that manganese is reduced to Mn^{2+} during hydrothermal synthesis and incorporated into the silicalite-2 framework during calcination at 500 °C. Further calcination at 750 °C does not affect the crystallinity but oxidizes essentially all of the Mn^{2+} to Mn^{3+} in the framework [392].

7. Conclusions

X-ray absorption spectroscopy is a versatile tool to determine the local structure of hetero-atoms in zeolites. Theoretical interpretation of spectra has been achieved to very high level of agreement with experiment, which has greatly helped interpretation of experimental spectra that have no counterpart in spectral data-bases. The ability of in situ measurement has been exploited and both the near-edge (XANES) and full range (EXAFS) data have been exploited. As a result, the changes in structure, both electronic and coordination of hetero-atoms in zeolites has been determined to great extent under pre-treatment and catalytically relevant conditions.
In this review we have deeply discussed the role of X-ray absorption spectroscopy in determining the structural and electronic configuration of heteroatoms in zeolites, barely

mentioning AlPOs and SAPO's systems for sake of brevity and certainly not for lack of interest. For each specific heteroatom, we mentioned the relevant support obtained by parallel techniques such as vibrational (IR and Raman), electronic (UV-Vis and XPS) and spin resonance (EPR and solid state NMR) spectroscopies. The intrinsic element sensitivity of the XAS technique has been identified as the more important aspect of this technique applied to characterize diluted species such as heteroatoms in zeolites. The main drawback of the technique, i.e. the averaging of all species present in the sample, has been discussed and clearly evidenced in the examples of Fe- and Ga-zeolites activated at high temperature. In those examples the superimposition of signals coming from the residual tetrahedral framework species and from several heterogeneous extra framework species resulted in an overall EXAFS signal of low intensity and of impossible disentanglement into the different single components.
Because still relatively young, X-ray emission spectroscopy (XES) [109, 355, 356, 393-395], has not been considered in this review. However, from the already limited published literature [108, 112, 133, 341, 342, 396-399] we foresee that XES will play a relevant role in the near future in determining the symmetry, coordination and ligand nature of metal centers in zeolites, zeotypes, and porous materials in general.

Acknowledgements
This review work has been realized within the MaMASELF framework (http://www.mamaself.eu/). CL thanks the support from the Mega-grant of the Russian Federation Government to economical supports of "Progetti di Ricerca di Ateneo-Compagnia di San Paolo-2011- Linea 1", ORTO11RRT5 project and of the scientific research at Southern Federal University, No.14.Y26.31.0001.

Scheme 1. Local environments of heteroatoms hosted in zeolitic frameworks. Part (a): M^{3+} heteroatoms induces a negative charge to the framework and experience a T_d-like environment with four equivalent M–O distances when the framework charge is balanced by NH_4 ion, by the template molecule or an alkali-metal cation (left part). When the charge is balanced by a proton (Brønsted site) then the M–O distance bearing the Brønsted site, M–(OH)–Si is significantly elongated with respect to the M–O distance of the remaining three M–O–Si bonds (right part). Vide infra Sections 2, 3 and 4.1. Part (b): M^{4+} heteroatoms do not induce any charge to the framework, they doesn't imply the presence of a charge balancing cation or Brønsted site and in vacuum-activated materials experience a T_d-like environment with four equivalent M–O distances. Upon interaction with ligands (L = H_2O or NH_3) Ti modifies its local environment coordinating one ligand molecule in its first coordination sphere. Vide infra Section 5 and Figure 8. Part (c): V^{5+} heteroatom links with only three framework oxygen atoms forming three equivalent V–O–Si bonds and with and oxygen atom via a double bond, experiencing a C_{3v} local environment. See Table 4 for a selection of M–O distances obtained by M K-edge EXAFS in the three different cases.

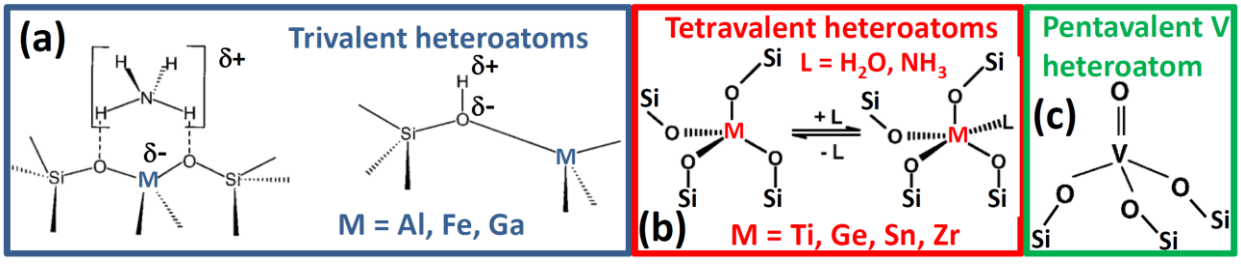

Figure 1. Part of the crystal structure of zeolite ZSM-5: Red bridging oxygen atoms; yellow silicon atoms; purple aluminum atoms. The large blue sphere identifies a ten-membered ring.

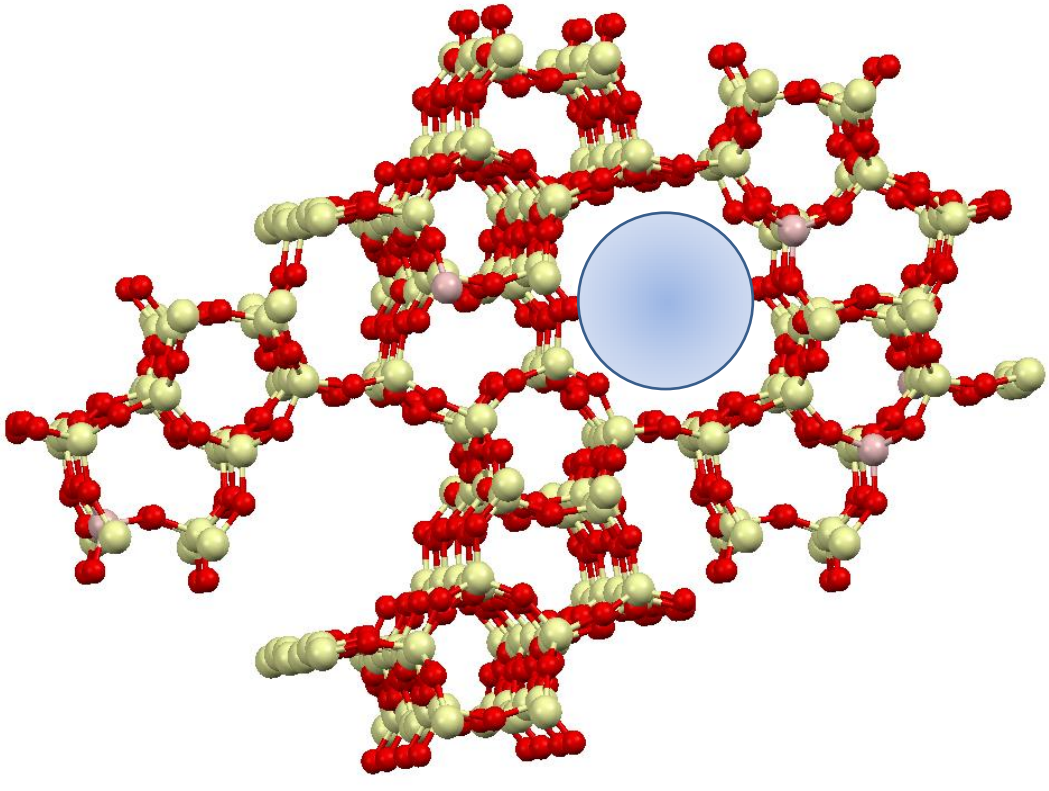

Figure 2. Part (A): Experimental Al K-edge XANES spectra of several materials possessing non-distorted or distorted octahedral Al sites. From top to bottom $YAlO_3$ perovskite [150]; topaz [400]; kayanite [400]; jadeite (dotted curve from Ref. [400], solid curve from Ref. [140]); and corundum [142]. Part (B): Al K-edge XANES spectra of several materials possessing tetrahedral Al sites. From top to bottom: Na^+-Y zeolite (experimental [155]); NH_4^+-Y zeolite (experimental [155]); albite [150]; AlO_4 cluster in T_d symmetry (FEFF6 calculation [150]). Adapted with permission from Ref. [150], copyright American Chemical Society 1999.

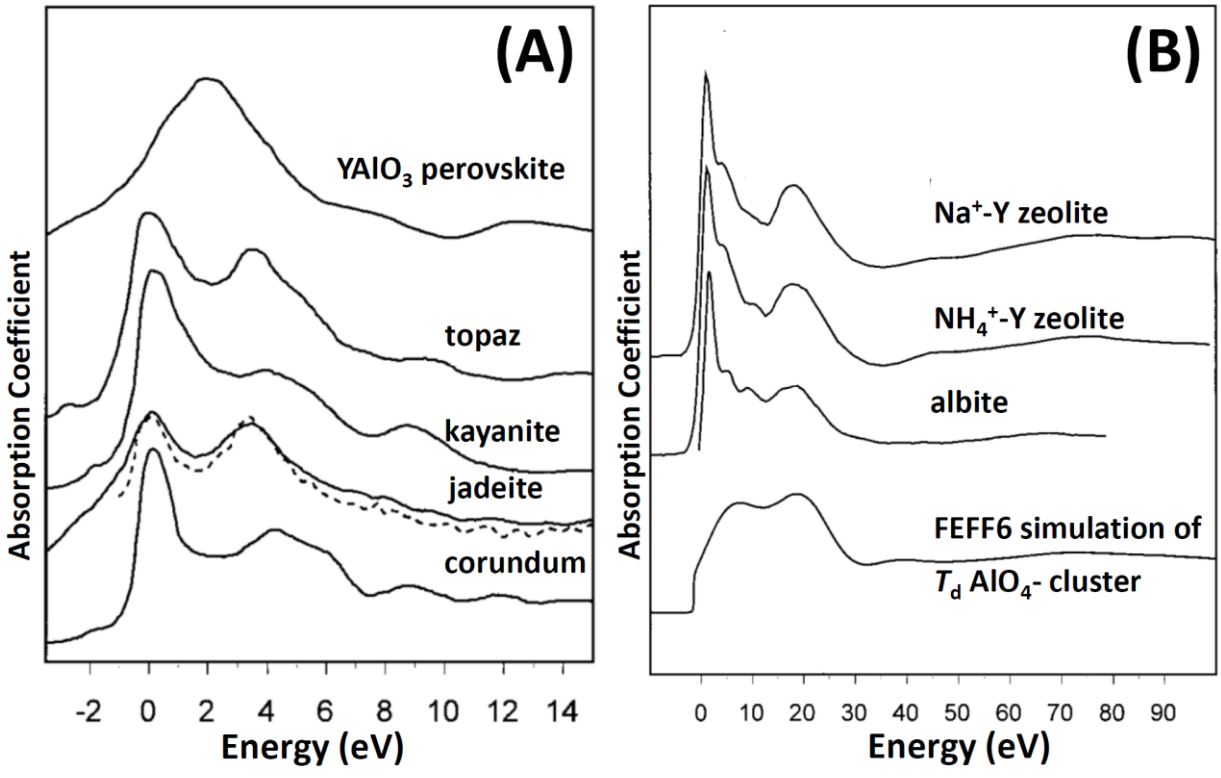

Figure 3. Schematic drawing of the 'ILEXAFS' cell, designed for in situ soft X-ray measurements. From top to bottom: the top flange (C), the reaction chamber (B) and the external cubic container (A). A hollow sphere is kept in place by two holders that contain X-ray transparent windows. Sample holder (S) can be cooled or heated, providing a working interval from 77 to 1000 K.

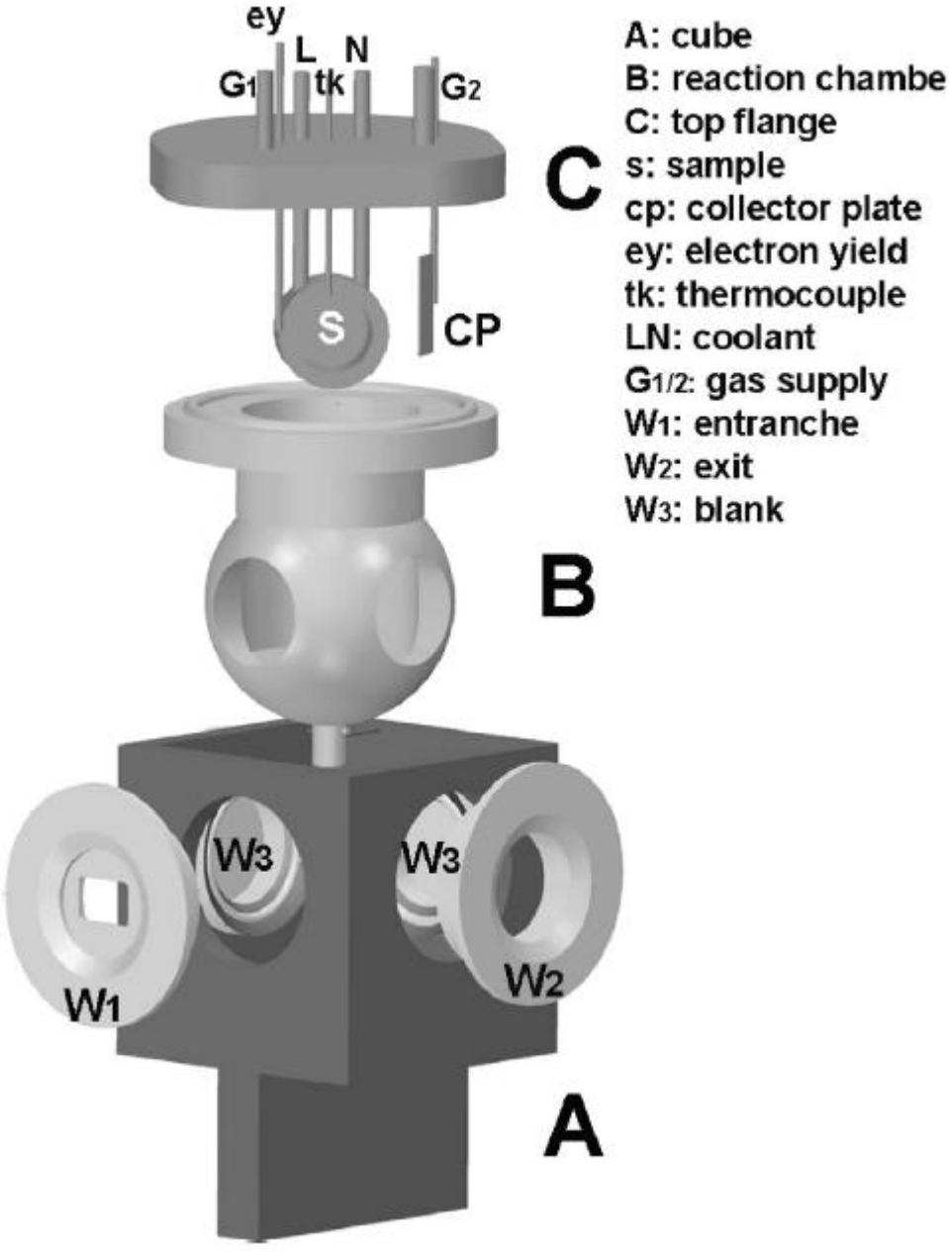

Figure 4. Asymmetry in the local structure of the catalytically active site during oligomerization of olefins. Compared to H Y zeolite, the asymmetry is lower, because of reaction of an intermediate with the acidic hydroxyl, shortening the longest Al – O bond.

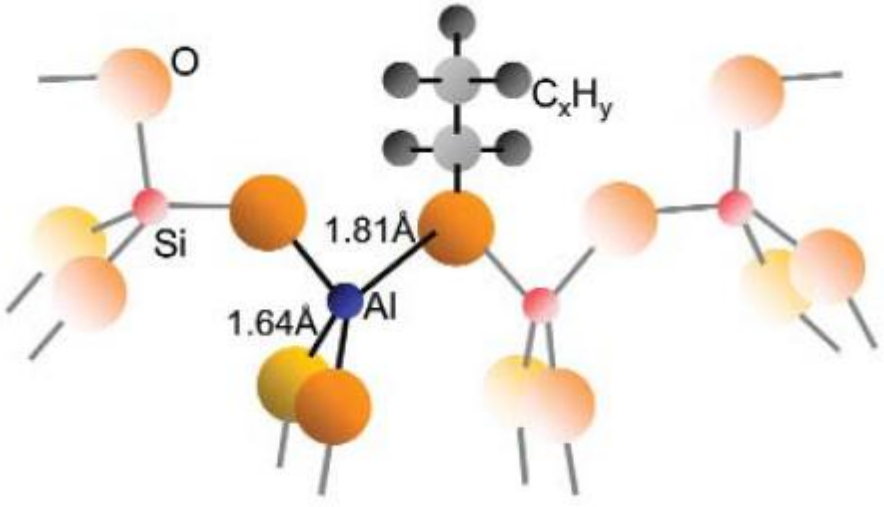

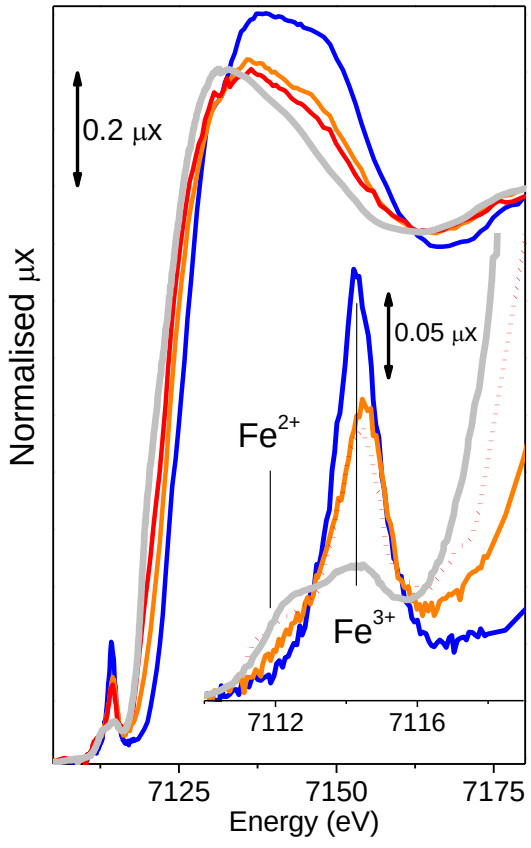

Figure 5. Fe K-edge XANES spectra of Fe-MFI (Si/Al = 90) with template (blue line), and activated at 773 K (orange line), and 973 K (red line). The gray spectrum corresponds to a different Fe-MFI sample (Si/Al = 68) activated at 1073 K. The inset reports the magnification of the pre-edge peak. Vertical lines represent the typical position for the pre-edge features of Fe^{2+} and Fe^{3+} species. The figure contains the experimental data published in Refs. [190, 206].

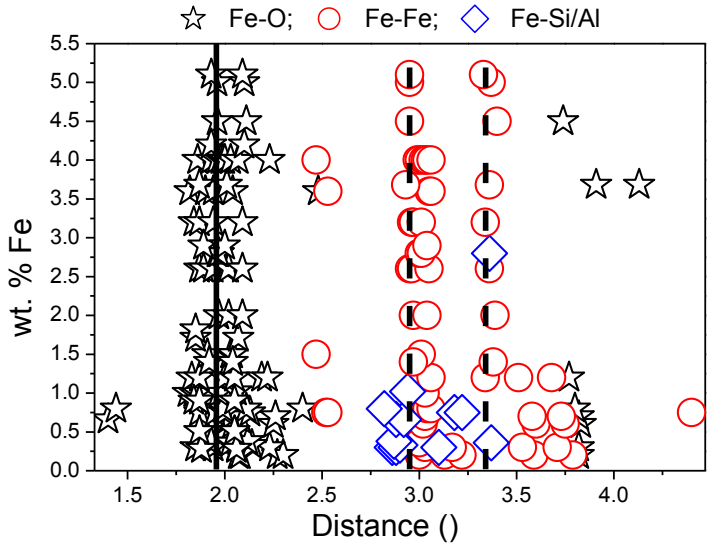

Figure 6. Summary of the diverse Fe–O (open square), Fe–Fe (open circle) and Fe–Si/Al (open triangle) distances calculated in the literature on the basis of EXAFS data. Distances are reported as a function of iron content. Full and dashed vertical lines indicate average Fe–O and Fe–Fe distances, respectively, obtained from XRD refinement of α-Fe_2O_3 (1.95, 2.96 and 3.34 Å). Reported data have been collected from refs. [176-196]. This figure represents an updated version of that published in Ref. [26].

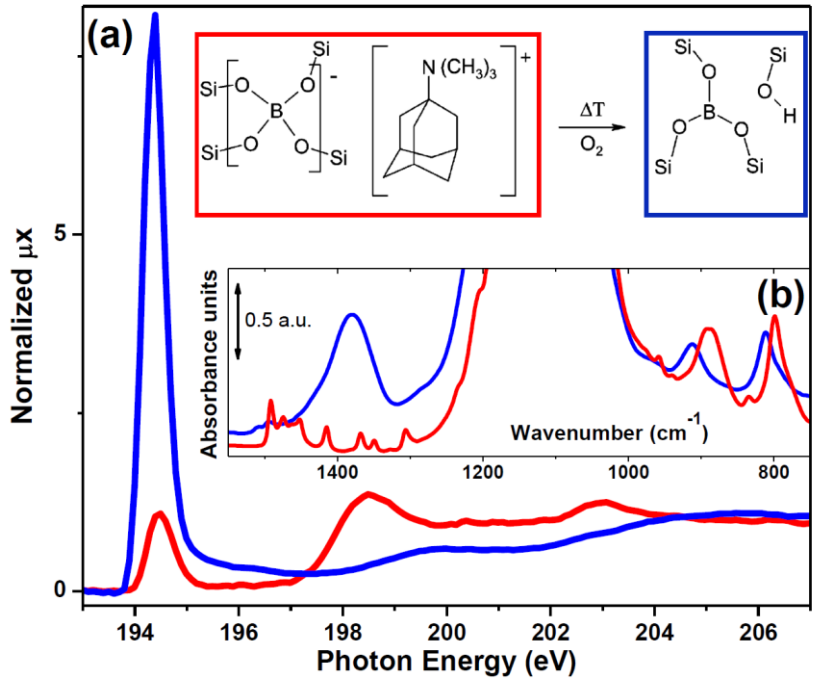

Figure 7. Part (a): Normalized B K-edge XAES spectra of B-SSZ-13 in presence of template (red curve), after calcination (blue curve). Part (b): same experiment followed by FTIR spectroscopy. Insets are used to reproduce the B species responsible for the XANES and IR spectra reported in parts (a) and (b), same color code. Unpublished figure reporting spectra published in Refs. [272, 274].

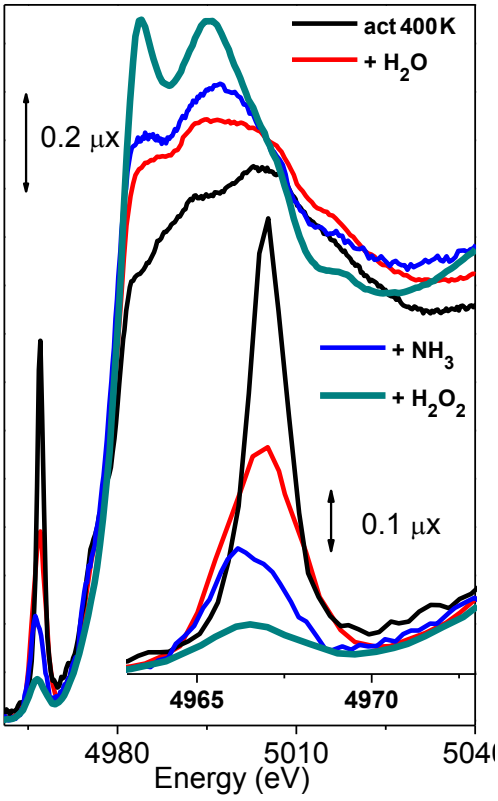

Figure 8. Effect of interaction with molecules of increasing interaction strength with Ti(IV) sites in TS-1 monitored by Ti K-edge XANES: water (red), ammonia (blue) and hydrogen peroxide (yellow). For comparison also the spectrum of the TS-1 dehydrated at 400 K has been reported (black). See also Scheme 1b. Unpublished figure reporting spectra published in Refs. [310, 320].

Table 1. Characteristic spectral features to distinguish aluminum coordination from Al K-edge XAS. ND = not determined. Adapted from Ref. [139].

Coordination	*Edge energy (eV)*	*Whiteline intensity*	*Characteristic peaks (eV)*[a]	*Pre-edge?*
Tetrahedral	1566	Low	20 & 70	No
Octahedral	1570	High	50	No
Distorted octahedral	1568	High and split	50	Small
Square planar	ND	Medium	ND	Large
Three coordinate	1566	low	ND	Large

[a] indicative of Al–O bond length

Table 2. Local structure of the framework aluminum in zeolites Na Y, H Y, and H-ZSM-5 based on Al K-edge EXAFS fitting (DWF = Debye-Waller factor). Reproduced from Ref. [157].

Na Y zeolite	**R / Å**	**DWF/Å^2**
Al – O	1.74	0.006
Al – O	1.74	0.006
Al – O	1.74	0.006
Al – O	1.74	0.006
Al – Na	3.15	0.016
Al – Si	3.12	0.016
H Y zeolite		
Al – O	1.68	0.006
Al – O	1.68	0.006
Al – O	1.68	0.006
Al – O(H)	1.87	0.006
Al – Si average	3.11	0.016
H ZSM-5		
Al – O	1.66	0.006
Al – O	1.71	0.006
Al – O	1.74	0.006
Al – O(H)	1.98	0.006
Al – Si average	3.09	0.016
Al – Si long	3.28	0.016

Table 3. Local structure of the framework aluminum in zeolite Y before, during and after reaction with ethylene based on Al K-edge EXAFS fitting; NH_4 Y, H Y, H Y during reaction and adsorption of a reactive intermediate, and H Y after desorption of the reactive intermediate. (DWF = Debye-Waller factor). Adapted from ref. [156].

NH_4 Y zeolite	**Coordination number (fitted value)**	**R / Å**	**DWF/Å^2**
Al – O	4.4	1.68	0.000[a]
H Y zeolite			
Al – O	3.1	1.66	-0.005
Al – O(H)	1.1	1.89	idem.
H Y zeolite reacting with $C_2^=$			
Al – O	3.4	1.64	-0.004
Al – O(H)	3.1	1.81	idem.
H Y zeolite after reaction with $C_2^=$			
Al – O	2.9	1.65	-0.008
Al – O(H)	1.1	1.91	idem.

[a] relative to the used reference

Table 4. Selection of M-O average distances for different heteroatom (M) insertion in different zeolitic frameworks. NPD = neutron powder diffraction; SC = single crystal; SR = synchrotron radiation; TPAOH = Tetrapropyl ammonium hydroxide (template molecule for MFI); TEAOH = Tetraethylammonium hydroxide (template molecule for BEA). All EXAFS data have been collected at the heteroatom K edge. For comparison, also the average Si–O distance in Al-free silicalite-1 as obtained by diffraction methods is reported. R_M represents the ionic radius of the M cation in tetrahedral coordination according to the compilation of Shannon [401]. Unpublished table.

M^{n+}	Hosting framework	R_M Å	R_M/R_{Si}	Technique	$< d_{M-O} >$ Å	Comment	Ref.
Si^{4+}	MFI	0.26	1	NPD	1.601	Defective silicalite-1 (Si vacancies)	[86]
Si^{4+}	MFI	0.26	1	SC SR XRD	1.591	Defect-free silicalite-1	[365]
Al^{3+}	FAU	0.39	1.5	EXAFS	1.74	Na^+-Y (4 equivalent Si-O bonds)	[157]
Al^{3+}	FAU	0.39	1.5	EXAFS	1.74	NH_4^+-Y (4 equivalent Si-O bonds)	[156]
Al^{3+}	FAU	0.39	1.5	EXAFS	1.68 1.87	H^+-Y (3 Al-O-Si bonds) H^+-Y (1 Al-OH-Si bond)	[157]
Al^{3+}	FAU	0.39	1.5	EXAFS	1.66 1.89	H^+-Y (3 Al-O-Si bonds) H^+-Y (1 Al-OH-Si bond)	[156]
Al^{3+}	MFI	0.39	1.5	EXAFS	1.70 1.98	H^+-ZSM-5 (Al-O-Si bonds) H^+-ZSM-5 (Al-OH-Si bond)	[157]
Fe^{3+}	MFI	0.49	1.885	EXAFS	1.85	$TPAOH^+$-Fe-silicalite-1 (4 equivalent Fe-O)	[195]
Fe^{3+}	MFI	0.49	1.885	EXAFS	1.86	NH_4^+-Fe-silicalite-1 (4 equivalent Fe-O)	[195]
Fe^{3+}	MFI	0.49	1.885	EXAFS	1.865 2.10	H^+-Fe-silicalite-1 (3 Fe-O-Si bonds) H^+-Fe-silicalite-1 (1 Fe-OH-Si bond)	[195]
Fe^{3+}	MWW	0.49	1.885	EXAFS	1.87	Fe-MCM-22 with template (4 equivalent Fe-O)	[219]
Fe^{3+}	LTL	0.49	1.885	EXAFS	1.85	Fe-LTL	[197]
Fe^{3+}	MOR	0.49	1.885	EXAFS	1.86	Fe-MOR	[198]
Ga^{3+}	MFI	0.47	1.808	EXAFS	1.82	$TPAOH^+$-Ga-ZSM-5 (4 equivalent Ga-O bonds)	[263]
Ga^{3+}	MFI	0.47	1.808	EXAFS	1.806	$TPAOH^+$-Ga-ZSM-5 (4 equivalent Ga-O bonds)	[266]
Ga^{3+}	MFI	0.47	1.808	EXAFS	1.809	NH_4^+-Ga- ZSM-5 (4 equivalent Ga-O bonds)	[266]
Ga^{3+}	MFI	0.47	1.808	EXAFS	1.80 2.02	H^+-Ga- ZSM-5 (3 Fe-O-Si bonds) H^+-Ga- ZSM-5 (1 Fe-OH-Si bond)	[266]
Ga^{3+}	BEA	0.47	1.808	EXAFS	1.80	Ga-β	[264]
Ga^{3+}	MOR	0.47	1.808	EXAFS	1.80	Na^+-Ga-MOR	[265]
Ga^{3+}	MOR	0.47	1.808	EXAFS	1.83	H^+-Ga-MOR	[265]
Ga^{3+}	BEA	0.47	1.808	EXAFS	1.807	$TPEOH^+$-Ga-β (4 equivalent Ga-O bonds)	[266]
Ga^{3+}	BEA	0.47	1.808	EXAFS	1.812	NH_4^+-Ga-β (4 equivalent Ga-O bonds)	[266]
Ga^{3+}	BEA	0.47	1.808	EXAFS	1.79 1.99	H^+-Ga-β (3 Fe-O-Si bonds) H^+-Ga-β (1 Fe-OH-Si bond)	[266]
Ti^{4+}	MFI	0.42	1.615	EXAFS	1.81	TS-1 (activated in vacuo)	[309]
Ti^{4+}	BEA	0.42	1.615	EXAFS	1.81	Ti-β (activated in vacuo)	[323]
Ti^{4+}	STT	0.42	1.615	EXAFS	1.84	Ti-STT (activated in vacuo)	[107, 329]
Ti^{4+}	CHA	0.42	1.615	EXAFS	1.81	Ti-SSZ-13 (activated in vacuo)	[107, 330]
Ge^{4+}	MFI	0.39	1.615	EXAFS	1.75	Ge-ZSM-5 (with template)	[357]
Ge^{4+}	MFI	0.39	1.615	EXAFS	1.72	Ge-ZSM-5 (after calcination)	[357]
Sn^{4+}	BEA	0.55	2.115	EXAFS	1.906	Sn-β	[359]
V^{5+}	MFI	0.355	1.365	EXAFS	1.68 1.78	VS-1 (1 V=O bond) VS-1 (3 V-O-Si bonds)	[383]
V^{5+}	BEA	0.355	1.365	EXAFS	1.64 1.73	VS-2 (1 V=O bond) VS-2 (3 V-O-Si bonds)	[378]

References

[1] R.M. Szostak, Molecular Sieves, Van Nostrand Reinhold, New York, 1989.
[2] M.E. Davis, Nature. 417 (2002) 813-821.
[3] A. Stein, Adv. Mater. 15 (2003) 763-775.
[4] W.M. Meier, D.H. Olson, C. Baerlocher, Atlas of Zeolite Structure Types, Elsevier, London, 1996.
[5] C.S. Cundy, P.A. Cox, Microporous Mesoporous Mat. 82 (2005) 1-78.
[6] W.M.H. Sachtler, Z.C. Zhang, Adv. Catal. 39 (1993) 129-220.
[7] L. Tosheva, V.P. Valtchev, Chem. Mat. 17 (2005) 2494-2513.
[8] A.F. Masters, T. Maschmeyer, Microporous and Mesoporous Materials. 142 (2011) 423-438.
[9] X.J. Meng, F.S. Xiao, Chem. Rev. 114 (2014) 1522-1544.
[10] S.L. Suib, Chem. Rev. 93 (1993) 803-826.
[11] B. Sulikowski, Heterogeneous Chem. Rev. 3 (1996) 203-268.
[12] Z. Gabelica, S. Valange, Microporous Mesoporous Mater. 30 (1999) 57-66.
[13] F.T. Fan, Z.C. Feng, C. Li, Accounts Chem. Res. 43 (2010) 378-387.
[14] Y. Ma, W. Tong, H. Zhou, S.L. Suib, Microporous Mesoporous Mater. 37 (2000) 243-252.
[15] R. Millini, G. Perego, G. Bellussi, Top. Catal. 9 (1999) 13-34.
[16] P. Ratnasamy, R. Kumar, Catal. Today. 9 (1991) 329-416.
[17] M.G. Clerici, in: S.D. Jackson, H.J.S. J. (Eds.), Metal Oxide Catalysis, Wiley-VCH Verlag GmbH & Co. KGaA, Weinheim, 2009, pp. 705-754.
[18] I. Arends, R.A. Sheldon, M. Wallau, U. Schuchardt, Angew. Chem.-Int. Edit. 36 (1997) 1144-1163.
[19] R.J. Francis, D. O'Hare, J. Chem. Soc.-Dalton Trans. (1998) 3133-3148.
[20] M. Hunger, Solid State Nucl. Magn. Reson. 6 (1996) 1-29.
[21] H. Knozinger, S. Huber, J. Chem. Soc.-Faraday Trans. 94 (1998) 2047-2059.
[22] A. Zecchina, G. Spoto, S. Bordiga, Physical Chemistry Chemical Physics. 7 (2005) 1627-1642.
[23] C. Lamberti, E. Groppo, G. Spoto, S. Bordiga, A. Zecchina, Adv. Catal. 51 (2007) 1-74.
[24] C. Lamberti, A. Zecchina, E. Groppo, S. Bordiga, Chem. Soc. Rev. 39 (2010) 4951-5001.
[25] B. Notari, Adv. Catal. 41 (1996) 253-334
[26] A. Zecchina, M. Rivallan, G. Berlier, C. Lamberti, G. Ricchiardi, Physical Chemistry Chemical Physics. 9 (2007) 3483-3499.
[27] A. Zecchina, C. Lamberti, S. Bordiga, Catal. Today. 41 (1998) 169-177.
[28] S. Bordiga, B. Civalleri, G. Spoto, C. Paze, C. Lamberti, P. Ugliengo, A. Zecchina, J. Chem. Soc.-Faraday Trans. 93 (1997) 3893-3898.
[29] C. Paze, S. Bordiga, C. Lamberti, M. Salvalaggio, A. Zecchina, G. Bellussi, J. Phys. Chem. B. 101 (1997) 4740-4751.
[30] C. Paze, S. Bordiga, G. Spoto, C. Lamberti, A. Zecchina, J. Chem. Soc.-Faraday Trans. 94 (1998) 309-314.
[31] L. Karwacki, M.H.F. Kox, D.A.M. de Winter, M.R. Drury, J.D. Meeldijk, E. Stavitski, W. Schmidt, M. Mertens, P. Cubillas, N. John, A. Chan, N. Kahn, S.R. Bare, M. Anderson, J. Kornatowski, B.M. Weckhuysen, Nat. Mater. 8 (2009) 959-965.
[32] M. Bjorgen, F. Bonino, S. Kolboe, K.P. Lillerud, A. Zecchina, S. Bordiga, J. Am. Chem. Soc. 125 (2003) 15863-15868.
[33] U. Olsbye, M. Bjorgen, S. Svelle, K.P. Lillerud, S. Kolboe, Catal. Today. 106 (2005) 108-111.
[34] U. Olsbye, S. Svelle, M. Bjorgen, P. Beato, T.V.W. Janssens, F. Joensen, S. Bordiga, K.P. Lillerud, Angew. Chem.-Int. Edit. 51 (2012) 5810-5831.
[35] S. Svelle, F. Joensen, J. Nerlov, U. Olsbye, K.P. Lillerud, S. Kolboe, M. Bjorgen, J. Am. Chem. Soc. 128 (2006) 14770-14771.
[36] J. Cejka, G. Centi, J. Perez-Pariente, W.J. Roth, Catal. Today. 179 (2012) 2-15.
[37] J.N. Armor, Chem. Mat. 6 (1994) 730-738.

[38] K. Komnitsas, D. Zaharaki, Miner. Eng. 20 (2007) 1261-1277.
[39] C. Martinez, A. Corma, Coord. Chem. Rev. 255 (2011) 1558-1580.
[40] B. Smit, T.L.M. Maesen, Nature. 451 (2008) 671-678.
[41] K. Tanabe, W.F. Holderich, Appl. Catal. A-Gen. 181 (1999) 399-434.
[42] P. Ungerer, Oil Gas Sci. Technol. 58 (2003) 271-297.
[43] W. Vermeiren, J.P. Gilson, Top. Catal. 52 (2009) 1131-1161.
[44] M. Al-Sabawi, J.W. Chen, S. Ng, Energy Fuels. 26 (2012) 5355-5372.
[45] H.S. Cerqueira, G. Caeiro, L. Costa, F.R. Ribeiro, J. Mol. Catal. A-Chem. 292 (2008) 1-13.
[46] G.W. Huber, A. Corma, Angew. Chem.-Int. Edit. 46 (2007) 7184-7201.
[47] A. Philippaerts, S. Goossens, W. Vermandel, M. Tromp, S. Turner, J. Geboers, G. Van Tendeloo, P.A. Jacobs, B.F. Sels, ChemSusChem. 4 (2011) 757-767.
[48] A. Zecchina, S. Bordiga, J.G. Vitillo, G. Ricchiardi, C. Lamberti, G. Spoto, M. Bjorgen, K.P. Lillerud, J. Am. Chem. Soc. 127 (2005) 6361-6366.
[49] L. Regli, A. Zecchina, J.G. Vitillo, D. Cocina, G. Spoto, C. Lamberti, K.P. Lillerud, U. Olsbye, S. Bordiga, Physical Chemistry Chemical Physics. 7 (2005) 3197-3203.
[50] T. Kerr G, in: W.M. Meier, J.B. Uytterhoeven (Eds.), Molecular Sieves, ACS, 1973, pp. 219-229.
[51] G. Yang, Current Catal. 3 (2014) 2-15.
[52] G.I. Panov, G.A. Sheveleva, A.S. Kharitonov, V.N. Romannikov, L.A. Vostrikova, Appl. Catal. A-Gen. 82 (1992) 31-36.
[53] A.S. Kharitonov, G.A. Sheveleva, G.I. Panov, V.I. Sobolev, Y.A. Paukshtis, V.N. Romannikov, Appl. Catal. A-Gen. 98 (1993) 33-43.
[54] X.B. Feng, W.K. Hall, J. Catal. 166 (1997) 368-376.
[55] E. Kikuchi, K. Yogo, S. Tanaka, M. Abe, Chem. Lett. (1991) 1063-1066.
[56] E.M. El-Malki, R.A. van Santen, W.M.H. Sachtler, Microporous Mesoporous Mat. 35-6 (2000) 235-244.
[57] Q. Zhu, B.L. Mojet, R.A.J. Janssen, E.J.M. Hensen, J. van Grondelle, P.C.M.M. Magusin, R.A. van Santen, Catal. Lett. 81 (2002) 205-212.
[58] G.D. Pirngruber, J. Catal. 219 (2003) 456-463.
[59] P.K. Roy, G.D. Pirngruber, J. Catal. 227 (2004) 164-174.
[60] J. Perez-Ramirez, F. Kapteijn, A. Bruckner, J. Catal. 218 (2003) 234-238.
[61] J. Perez-Ramirez, M.S. Kumar, A. Bruckner, J. Catal. 223 (2004) 13-27.
[62] http://www.iza-structure.org/databases/.
[63] R. Szostak, T.L. Thomas, J. Catal. 100 (1986) 555-557.
[64] A.K. Cheetham, A.P. Wilkinson, Angew. Chem.-Int. Edit. Engl. 31 (1992) 1557-1570.
[65] T. Armbruster, M.E. Gunter, in: D.L. Bish, D.W. Ming (Eds.), Natural Zeolites: Occurrence, Properties, Applications, Mineralogical Soc Amer, Chantilly, 2001, pp. 1-67.
[66] A.W. Burton, Z. Kristall. 219 (2004) 866-880.
[67] A.W. Burton, Powder Diffraction in Zeolite Science An Introductory Guide, Springer-Verlag Berlin, Berlin, 2009.
[68] P. Demontis, G.B. Suffritti, Chem. Rev. 97 (1997) 2845-2878.
[69] T. Frising, P. Leflaive, Microporous Mesoporous Mater. 114 (2008) 27-63.
[70] H. Jobic, Curr. Opin. Solid State Mat. Sci. 6 (2002) 415-422.
[71] Z. Liu, N. Fujita, K. Miyasaka, L. Han, S.M. Stevens, M. Suga, S. Asahina, B. Slater, C.H. Xiao, Y. Sakamoto, M.W. Anderson, R. Ryoo, O. Terasaki, Microscopy. 62 (2013) 109-146.
[72] J. Marti-Rujas, M. Kawano, Accounts Chem. Res. 46 (2013) 493-505.
[73] L.B. McCusker, C. Baerlocher, Z. Kristall. 228 (2013) 1-10.
[74] M.G. O'Brien, A.M. Beale, B.M. Weckhuysen, Chem. Soc. Rev. 39 (2010) 4767-4782.
[75] F.R. Trouw, D.L. Price, Annu. Rev. Phys. Chem. 50 (1999) 571-601.
[76] T. Willhammar, X.D. Zou, Z. Kristall. 228 (2013) 11-27.

[77] S. Smeekens, S. Heylen, K. Villani, K. Houthoofd, E. Godard, M. Tromp, J.W. Seo, M. DeMarco, C.E.A. Kirschhock, J.A. Martens, Chem. Sci. 1 (2010) 763-771.
[78] Y. Liu, W.Z. Zhang, T.J. Pinnavaia, J. Am. Chem. Soc. 122 (2000) 8791-8792.
[79] Y. Liu, W.Z. Zhang, T.J. Pinnavaia, Angew. Chem.-Int. Edit. 40 (2001) 1255-1258.
[80] L.R. Aramburo, S. Teketel, S. Svelle, S.R. Bare, B. Arstad, H.W. Zandbergen, U. Olsbye, F.M.F. de Groot, B.M. Weckhuysen, J. Catal. 307 (2013) 185-193.
[81] J.A. van Bokhoven, M. Tromp, D.C. Koningsberger, J.T. Miller, J.A.Z. Pieterse, J.A. Lercher, B.A. Williams, H.H. Kung, J. Catal. 202 (2001) 129-140.
[82] S. van Donk, A.H. Janssen, J.H. Bitter, K.P. de Jong, Catal. Rev.-Sci. Eng. 45 (2003) 297-319.
[83] I. Arends, R.A. Sheldon, Appl. Catal. A-Gen. 212 (2001) 175-187.
[84] J. Gopalakrishnan, Chem. Mat. 7 (1995) 1265-1275.
[85] U. Schuchardt, D. Cardoso, R. Sercheli, R. Pereira, R.S. de Cruz, M.C. Guerreiro, D. Mandelli, E.V. Spinace, E.L. Fires, Appl. Catal. A-Gen. 211 (2001) 1-17.
[86] G. Artioli, C. Lamberti, G.L. Marra, Acta Cryst. B. 56 (2000) 2-10.
[87] S. Bordiga, I. Roggero, P. Ugliengo, A. Zecchina, V. Bolis, G. Artioli, R. Buzzoni, G.L. Marra, F. Rivetti, G. Spanò, C. Lamberti, J. Chem. Soc. Dalton Trans. (2000) 3921-3929.
[88] S. Bordiga, P. Ugliengo, A. Damin, C. Lamberti, G. Spoto, A. Zecchina, G. Spanò, R. Buzzoni, L. Dalloro, F. Rivetti, Top. Catal. 15 (2001) 43-52.
[89] J.A. van Bokhoven, A.L. Roest, D.C. Koningsberger, J.T. Miller, G.H. Nachtegaal, A.P.M. Kentgens, J. Phys. Chem. B. 104 (2000) 6743-6754.
[90] W.-C. Yang, Handbook of Fluidization and Fluid Particle Systems, Taylor & Francis, New York, 2005.
[91] C.R. Moreira, N. Homs, J.L.G. Fierro, M.M. Pereira, P.R. de la Piscina, Microporous Mesoporous Mat. 133 (2010) 75-81.
[92] W.H. Yateem, V. Nassehi, A.R. Khan, Water Air Soil Pollut. 218 (2011) 37-47.
[93] Y.M. Zhang, C.R. Xiong, Catal. Sci. Technol. 2 (2012) 606-612.
[94] J. Klinowski, Chem. Rev. 91 (1991) 1459-1479.
[95] W.P. Zhang, S.T. Xu, X.W. Han, X.H. Bao, Chem. Soc. Rev. 41 (2012) 192-210.
[96] H. Koller, M. Weiss, in: J.C.C. Chan (Ed.), Solid State Nmr, Springer-Verlag Berlin, Berlin, 2012, pp. 189-227.
[97] L. Mafra, J.A. Vidal-Moya, T. Blasco, Annu. Rep. NMR Spectrosc. 77 (2012) 259-351.
[98] S.H. Li, F. Deng, Annu. Rep. NMR Spectrosc. 78 (2013) 1-54.
[99] M. Hunger, Catal. Rev.-Sci. Eng. 39 (1997) 345-393.
[100] W.E. Farneth, R.J. Gorte, Chem. Rev. 95 (1995) 615-635.
[101] J. Klinowski, T.L. Barr, Accounts Chem. Res. 32 (1999) 633-640.
[102] M.E. Smith, Appl. Magn. Reson. 4 (1993) 1-64.
[103] A. Vimont, F. Thibault-Starzyk, M. Daturi, Chem. Soc. Rev. 39 (2010) 4928-4950.
[104] G. Spoto, S. Bordiga, A. Zecchina, D. Cocina, E.N. Gribov, L. Regli, E. Groppo, C. Lamberti, Catal. Today. 113 (2006) 65-80.
[105] Y. Okamoto, Crit. Rev. Surf. Chem. 5 (1995) 249-274.
[106] M. Stocker, Microporous Mater. 6 (1996) 235-257.
[107] S. Bordiga, E. Groppo, G. Agostini, J.A. van Bokhoven, C. Lamberti, Chem. Rev. 113 (2013) 1736-1850.
[108] C. Garino, E. Borfecchia, R. Gobetto, J.A. van Bokhoven, C. Lamberti, Coord. Chem. Rev. (2014) in press, http://dx.doi.org/10.1016/j.ccr.2014.1003.1027.
[109] L. Mino, G. Agostini, E. Borfecchia, D. Gianolio, A. Piovano, E. Gallo, C. Lamberti, J. Phys. D-Appl. Phys. 46 (2013) Art. n. 423001.
[110] C. Lamberti, Surf. Sci. Rep. 53 (2004) 1-197.

[111] F. Boscherini, in: C. Lamberti, G. Agostini (Eds.), Characterization of Semiconductor Heterostructures and Nanostructures (Second Edition), Elsevier, Amsterdam, 2013, pp. 259-310.
[112] F. Bonino, C. Prestipino, G. Agostini, A. Piovano, D. Gianolio, L. Mino, E. Gallo, C. Lamberti, in: F. Boscherini, C. Meneghini, S. Mobilio (Eds.), Synchrotron Radiation: Basics, Methods and Applications, Springer, Berlin, 2014.
[113] R. Prins, D.C. Koningsberger, in: D.C. Koningsberger, R. Prins (Eds.), X-Ray Absorption: Principles, Applications, Techniques of EXAFS, SEXAFS and XANES, John Wiley & Sons, New York, 1988, p. 321.
[114] R. Le Toquin, W. Paulus, A. Cousson, C. Prestipino, C. Lamberti, J. Am. Chem. Soc. 128 (2006) 13161-13174.
[115] A. Piovano, G. Agostini, A.I. Frenkel, T. Bertier, C. Prestipino, M. Ceretti, W. Paulus, C. Lamberti, J. Phys. Chem. C. 115 (2011) 1311-1322.
[116] C. Lamberti, C. Prestipino, F. Bonino, L. Capello, S. Bordiga, G. Spoto, A. Zecchina, S.D. Moreno, B. Cremaschi, M. Garilli, A. Marsella, D. Carmello, S. Vidotto, G. Leofanti, Angew. Chem. Int. Edit. 41 (2002) 2341-2344.
[117] N.B. Muddada, U. Olsbye, L. Caccialupi, F. Cavani, G. Leofanti, D. Gianolio, S. Bordiga, C. Lamberti, Physical Chemistry Chemical Physics. 12 (2010) 5605-5618.
[118] N.B. Muddada, U. Olsbye, G. Leofanti, D. Gianolio, F. Bonino, S. Bordiga, T. Fuglerud, S. Vidotto, A. Marsella, C. Lamberti, Dalton Trans. 39 (2010) 8437-8449.
[119] J.M. Bennett, W.J. Dytrych, J.J. Pluth, J.W. Richardson, J.V. Smith, Zeolites. 6 (1986) 349-360.
[120] A. Corma, M.J. Diaz-Cabanas, J.L. Jorda, C. Martinez, M. Moliner, Nature. 443 (2006) 842-845.
[121] M. Hartmann, L. Kevan, Chem. Rev. 99 (1999) 635-663.
[122] E.R. Parnham, R.E. Morris, Accounts Chem. Res. 40 (2007) 1005-1013.
[123] J.M. Thomas, Angew. Chem.-Int. Edit. 33 (1994) 913-937.
[124] J.M. Thomas, R. Raja, G. Sankar, R.G. Bell, Nature. 398 (1999) 227-230.
[125] J.H. Yu, R.R. Xu, Accounts Chem. Res. 36 (2003) 481-490.
[126] J.H. Yu, R.R. Xu, Chem. Soc. Rev. 35 (2006) 593-604.
[127] G. Mali, A. Ristic, V. Kaucic, J. Phys. Chem. B. 109 (2005) 10711-10716.
[128] N.N. Tusar, V. Kaucic, S. Geremia, G. Vlaic, Zeolites. 15 (1995) 708-713.
[129] A. Moen, D.G. Nicholson, M. Ronning, G.M. Lamble, J.F. Lee, H. Emerich, J. Chem. Soc.-Faraday Trans. 93 (1997) 4071-4077.
[130] I.L. Franklin, A.M. Beale, G. Sankar, Catal. Today. 81 (2003) 623-629.
[131] S. Cecowski, N.N. Tusar, M. Rangus, G. Mali, G. Soler-Illia, V. Kaucic, Microporous Mesoporous Mat. 135 (2010) 161-169.
[132] B.Y. Hsu, S. Cheng, J.M. Chen, J. Mol. Catal. A-Chem. 149 (1999) 7-23.
[133] E. Gallo, A. Piovano, C. Marini, O. Mathon, S. Pascarelli, P. Glatzel, C. Lamberti, G. Berlier, J. Phys. Chem. C (2014) submitted.
[134] P. Selvam, S.K. Mohapatra, J. Catal. 233 (2005) 276-287.
[135] G. Zadrozna, E. Souvage, J. Kornatowski, J. Catal. 208 (2002) 270-275.
[136] C.H. Lin, Y.C. Yang, C.Y. Chen, S.L. Wang, Chem. Mat. 18 (2006) 2095-2101.
[137] D. Cabaret, P. Sainctavit, P. Ildefonse, A.M. Flank, J. Phys.-Condes. Matter. 8 (1996) 3691-3704.
[138] L.A. Bugaev, P. Ildefonse, A.M. Flank, A.P. Sokolenko, H.V. Dmitrienko, J. Phys.-Condes. Matter. 10 (1998) 5463-5473.
[139] J.A. van Bokhoven, T. Nabi, H. Sambe, D.E. Ramaker, D.C. Koningsberger, J. Phys.-Condes. Matter. 13 (2001) 10247-10260.
[140] D.A. McKeown, G.A. Waychunas, G.E. Brown, J. Non-Cryst. Solids. 74 (1985) 349-371.
[141] G. Calas, G.E. Brown, G.A. Waychunas, J. Petiau, Phys. Chem. Miner. 15 (1987) 19-29.
[142] P. Ildefonse, R.J. Kirkpatrick, B. Montez, G. Calas, A.M. Flank, P. Lagarde, Clay Clay Min. 42 (1994) 276-287.

[143] C. Landron, M.C. Badets, A. Douy, J. Coutures, J.P. Coutures, P. Daniel, A.M. Flank, Phys. Status Solidi B-Basic Res. 167 (1991) 429-440.
[144] D.E. Li, G.M. Bancroft, M.E. Fleet, X.H. Feng, Y. Pan, Am. Miner. 80 (1995) 432-440.
[145] A. Mottana, A. Marcelli, G. Cibin, M.D. Dyar, Micas: Crystal Chemistry and Metamorphic Petrology. 46 (2002) 371-411.
[146] Z.Y. Wu, A. Marcelli, A. Mottana, G. Giuli, E. Paris, F. Seifert, Phys. Rev. B. 54 (1996) 2976-2979.
[147] A. Mottana, T. Murata, A. Marcelli, Z.Y. Wu, G. Cibin, E. Paris, G. Giuli, Phys. Chem. Miner. 27 (1999) 20-33.
[148] A. Mottana, J.L. Robert, A. Marcelli, G. Giuli, G. Della Ventura, E. Paris, Z.Y. Wu, Am. Miner. 82 (1997) 497-502.
[149] L. Bugaev, A. Sokolenko, D. Cabaret, P. Ildefonse, P. Sainctavit, J. Phys. IV. 7 (1997) 141-142.
[150] J.A. van Bokhoven, H. Sambe, D.E. Ramaker, D.C. Koningsberger, J. Phys. Chem. B. 103 (1999) 7557-7564.
[151] J.A. van Bokhoven, D.C. Koningsberger, P. Kunkeler, H. van Bekkum, J. Catal. 211 (2002) 540-547.
[152] C. Brouder, D. Cabaret, A. Juhin, P. Sainctavit, Phys. Rev. B. 81 (2010) Art. n. 115125.
[153] P. Ildefonse, D. Cabaret, P. Sainctavit, G. Calas, A.M. Flank, P. Lagarde, Phys. Chem. Miner. 25 (1998) 112-121.
[154] M. Fröba, J. Wong, P. Behrens, P. Sieger, M. Rowen, T. Tanaka, Z. Rek, J. Felsche, Physica B: Condens. Matter. 208–209 (1995) 65-67.
[155] D.C. Koningsberger, J.T. Miller, Catal. Lett. 29 (1994) 77-90.
[156] J.A. van Bokhoven, A.M.J. van der Eerden, R. Prins, J. Am. Chem. Soc. 126 (2004) 4506-4507.
[157] R.W. Joyner, A.D. Smith, M. Stockenhuber, M.W.E. van den Berg, Physical Chemistry Chemical Physics. 6 (2004) 5435-5439.
[158] U. Eichler, M. Brändle, J. Sauer, J. Phys. Chem. B. 101 (1997) 10035-10050.
[159] R. Duchateau, R.J. Harmsen, H.C.L. Abbenhuis, R.A. van Santen, A. Meetsma, S.K.H. Thiele, M. Kranenburg, Chem.–Euro. J. 5 (1999) 3130-3135.
[160] L.B. Alemany, R.L. Callender, A.R. Barron, S. Steuernagel, D. Iuga, A.P.M. Kentgens, J. Phys. Chem. B. 104 (2000) 11612-11616.
[161] J.A. van Bokhoven, A.M.J. van der Eerden, A.D. Smith, D.C. Koningsberger, J. Synchrotron Radiat. 6 (1999) 201-203.
[162] A.M.J. van der Eerden, J.A. van Bokhoven, A.D. Smith, D.C. Koningsberger, Rev. Sci. Instrum. 71 (2000) 3260-3266.
[163] I.J. Drake, Y.H. Zhang, M.K. Gilles, C.N.T. Liu, P. Nachimuthu, R.C.C. Perera, H. Wakita, A.T. Bell, J. Phys. Chem. B. 110 (2006) 11665-11676.
[164] G. Agostini, C. Lamberti, L. Palin, M. Milanesio, N. Danilina, B. Xu, M. Janousch, J.A. van Bokhoven, J. Am. Chem. Soc. 132 (2010) 667-678.
[165] J.O. Ehresmann, W. Wang, B. Herreros, D.-P. Luigi, T.N. Venkatraman, W. Song, J.B. Nicholas, J.F. Haw, J. Am. Chem. Soc. 124 (2002) 10868-10874.
[166] X. Rozanska, T. Demuth, F. Hutschka, J. Hafner, R.A. van Santen, J. Phys. Chem. B. 106 (2002) 3248-3254.
[167] R.W. Joyner, O. Sonntag, A.D. Smith, M. Stockenhuber, Stud. Surf. Sci. Catal. 170 (2007) 756-761.
[168] E. Bourgeat-Lami, P. Massiani, F. Direnzo, P. Espiau, F. Fajula, T.D. Courieres, Appl. Catal. 72 (1991) 139-152.
[169] B.H. Wouters, T.H. Chen, P.J. Grobet, J. Am. Chem. Soc. 120 (1998) 11419-11425.
[170] A. Omegna, J.A. van Bokhoven, R. Prins, J. Phys. Chem. B. 107 (2003) 8854-8860.
[171] A. Omegna, R. Prins, J.A. van Bokhoven, J. Phys. Chem. B. 109 (2005) 9280-9283.
[172] A. Abraham, S.-H. Lee, C.-H. Shin, S. Bong Hong, R. Prins, J.A. van Bokhoven, Physical Chemistry Chemical Physics. 6 (2004) 3031-3036.

[173] J.A. van Bokhoven, A.M.J. van der Eerden, D.C. Koningsberger, J. Am. Chem. Soc. 125 (2003) 7435-7442.
[174] L.A. Bugaev, J.A. van Bokhoven, A.P. Sokolenko, Y.V. Latokha, L.A. Avakyan, J. Phys. Chem. B. 109 (2005) 10771-10778.
[175] J.A. van Bokhoven, A.M.J. van der Eerden, D.C. Koningsberger, Stud. Surf. Sci. Catal. 142 (2002) 1885-1890.
[176] A.S. Krylov, J.F. Poliakoff, M. Stockenhuber, Physical Chemistry Chemical Physics. 2 (2000) 5743-5749.
[177] G.D. Pirngruber, P.K. Roy, N. Weiher, J. Phys. Chem. B. 108 (2004) 13746-13754.
[178] G.D. Pirngruber, M. Luechinger, P.K. Roy, A. Cecchetto, P. Smirniotis, J. Catal. 224 (2004) 429-440.
[179] G.D. Pirngruber, P.K. Roy, R. Prins, Physical Chemistry Chemical Physics. 8 (2006) 3939-3950.
[180] P. Marturano, L. Drozdova, A. Kogelbauer, R. Prins, J. Catal. 192 (2000) 236-247.
[181] P. Marturano, L. Drozdova, G.D. Pirngruber, A. Kogelbauer, R. Prins, Physical Chemistry Chemical Physics. 3 (2001) 5585-5595.
[182] R. Joyner, M. Stockenhuber, J. Phys. Chem. B. 103 (1999) 5963-5976.
[183] E.J.M. Hensen, Q. Zhu, M. Hendrix, A.R. Overweg, P.J. Kooyman, M.V. Sychev, R.A. van Santen, J. Catal. 221 (2004) 560-574.
[184] W.M. Heijboer, D.C. Koningsberger, B.M. Weckhuysen, F.M.F. de Groot, Catal. Today. 110 (2005) 228-238.
[185] F. Heinrich, C. Schmidt, E. Loffler, M. Menzel, W. Grünert, J. Catal. 212 (2002) 157-172.
[186] Y.Y. Ji, V. Koot, A.M.J. van der Eeirden, B.M. Weckhuysen, D.C. Koningsberger, D.E. Ramaker, J. Catal. 245 (2007) 415-427.
[187] S.H. Choi, B.R. Wood, J.A. Ryder, A.T. Bell, J. Phys. Chem. B. 107 (2003) 11843-11851.
[188] S.H. Choi, B.R. Wood, A.T. Bell, M.T. Janicke, K.C. Ott, J. Phys. Chem. B. 108 (2004) 8970-8975.
[189] M. Schwidder, M.S. Kumar, K. Klementiev, M.M. Pohl, A. Brückner, W. Grünert, J. Catal. 231 (2005) 314-330.
[190] G. Berlier, G. Spoto, P. Fisicaro, S. Bordiga, A. Zecchina, E. Giamello, C. Lamberti, Microchem. J. 71 (2002) 101-116.
[191] A.G. Popov, A.V. Smirnov, E.E. Knyazeva, V.V. Yuschenko, E.A. Kalistratova, K.V. Klementiev, W. Grunert, Ivanova, II, Microporous Mesoporous Mat. 134 (2010) 124-133.
[192] M. Hoj, M.J. Beier, J.D. Grunwaldt, S. Dahl, Appl. Catal. B-Environ. 93 (2009) 166-176.
[193] J. Janas, J. Gurgul, R.P. Socha, T. Shishido, M. Che, S. Dzwigaj, Appl. Catal. B-Environ. 91 (2009) 113-122.
[194] J.H. Park, J.H. Choung, I.S. Nam, S.W. Ham, Appl. Catal. B-Environ. 78 (2008) 342-354.
[195] S. Bordiga, R. Buzzoni, F. Geobaldo, C. Lamberti, E. Giamello, A. Zecchina, G. Leofanti, G. Petrini, G. Tozzola, G. Vlaic, J. Catal. 158 (1996) 486-501.
[196] S.M. Maier, A. Jentys, M. Janousch, J.A. van Bokhoven, J.A. Lercher, J. Phys. Chem. C. 116 (2012) 5846-5856.
[197] Y.S. Ko, W.S. Ahn, Microporous Mater. 9 (1997) 131-140.
[198] Y.S. Ko, H.T. Jang, W.S. Ahn, Korean J. Chem. Eng. 25 (2008) 1286-1291.
[199] A.A. Battiston, J.H. Bitter, F.M.F. de Groot, A.R. Overweg, O. Stephan, J.A. van Bokhoven, P.J. Kooyman, C. van der Spek, G. Vanko, D.C. Koningsberger, J. Catal. 213 (2003) 251-271.
[200] K.A. Dubkov, N.S. Ovanesyan, A.A. Shteinman, E.V. Starokon, G.I. Panov, J. Catal. 207 (2002) 341-352.
[201] J.M.M. Millet, Adv. Catal. 51 (2007) 309-350.
[202] J. Perez-Ramirez, G. Mul, F. Kapteijn, J.A. Moulijn, A.R. Overweg, A. Domenech, A. Ribera, I. Arends, J. Catal. 207 (2002) 113-126.
[203] L.H. Singh, R. Govindaraj, G. Amarendra, C.S. Sundar, Appl. Phys. Lett. 103 (2013) 5.
[204] A. Tuel, I. Arcon, J.M.M. Millet, J. Chem. Soc.-Faraday Trans. 94 (1998) 3501-3510.

[205] G. Berlier, G. Spoto, G. Ricchiardi, S. Bordiga, C. Lamberti, A. Zecchina, J. Mol. Catal. A-Chem. 182 (2002) 359-366.
[206] G. Berlier, G. Spoto, S. Bordiga, G. Ricchiardi, P. Fisicaro, A. Zecchina, I. Rossetti, E. Selli, L. Forni, E. Giamello, C. Lamberti, J. Catal. 208 (2002) 64-82.
[207] G. Berlier, A. Zecchina, G. Spoto, G. Ricchiardi, S. Bordiga, C. Lamberti, J. Catal. 215 (2003) 264-270.
[208] G. Berlier, F. Bonino, A. Zecchina, S. Bordiga, C. Lamberti, ChemPhysChem. 4 (2003) 1073-1078.
[209] G. Berlier, C. Lamberti, R. M., G. Mul, Physical Chemistry Chemical Physics. 12 (2010) 358-364.
[210] A. Zecchina, F. Geobaldo, C. Lamberti, S. Bordiga, G. Turnes Palomino, C. Otero Areán, Catal. Lett. 42 (1996) 25-33.
[211] M.S. Kumar, M. Schwidder, W. Grunert, A. Bruckner, J. Catal. 227 (2004) 384-397.
[212] A.M. Ferretti, C. Oliva, L. Forni, G. Berlier, A. Zecchina, C. Lamberti, J. Catal. 208 (2002) 83-88.
[213] F. Bonino, A. Damin, A. Piovano, C. Lamberti, S. Bordiga, A. Zecchina, ChemCatChem. 3 (2011) 139-142.
[214] S.A. Axon, K.K. Fox, S.W. Carr, J. Klinowski, Chem. Phys. Lett. 189 (1992) 1-6.
[215] S. Bordiga, F. Geobaldo, C. Lamberti, A. Zecchina, F. Boscherini, F. Genoni, G. Leofanti, G. Petrini, M. Padovan, S. Geremia, G. Vlaic, Nucl. Instr. Meth. B. 97 (1995) 23-27.
[216] A. Zecchina, S. Bordiga, C. Lamberti, G. Ricchiardi, C. Lamberti, G. Ricchiardi, D. Scarano, G. Petrini, G. Leofanti, M. Mantegazza, Catal. Today. 32 (1996) 97-106.
[217] D.W. Lewis, C.R.A. Catlow, G. Sankar, S.W. Carr, J. Phys. Chem. 99 (1995) 2377-2383.
[218] C. Lamberti, G. Turnes Palomino, S. Bordiga, D. Arduino, A. Zecchina, G. Vlaic, Jpn. J. Appl. Phys. Part 1. 38-1 (1999) 55-58.
[219] G. Berlier, M. Pourny, S. Bordiga, G. Spoto, A. Zecchina, C. Lamberti, J. Catal. 229 (2005) 45-54.
[220] G. Berlier, C. Prestipino, M. Rivallan, S. Bordiga, C. Lamberti, A. Zecchina, J. Phys. Chem. B. 109 (2005) 22377-22385.
[221] P. Marturano, A. Kogelbauer, R. Prins, J. Catal. 190 (2000) 460-468.
[222] A.A. Battiston, J.H. Bitter, D.C. Koningsberger, Catal. Lett. 66 (2000) 75-79.
[223] A.A. Battiston, J.H. Bitter, W.M. Heijboer, F.M.F. de Groot, D.C. Koningsberger, J. Catal. 215 (2003) 279-293.
[224] A.A. Battiston, J.H. Bitter, D.C. Koningsberger, J. Catal. 218 (2003) 163-177.
[225] E. Paris, A. Mottana, P. Mattias, Mineral. Petrol. 45 (1991) 105-117.
[226] E. Paris, T.A. Tyson, Phys. Chem. Miner. 21 (1994) 299-308.
[227] F. Farges, Phys. Chem. Miner. 22 (1995) 318-322.
[228] G. Giuli, E. Paris, Z.Y. Wu, M.F. Brigatti, G. Cibin, A. Mottana, A. Marcelli, Eur. J. Mineral. 13 (2001) 1099-1108.
[229] P.E. Petit, F. Farges, M. Wilke, V.A. Sole, J. Synchrot. Radiat. 8 (2001) 952-954.
[230] M. Wilke, F. Farges, P.E. Petit, G.E. Brown, F. Martin, Am. Miner. 86 (2001) 714-730.
[231] G. Giuli, E. Paris, Z.Y. Wu, A. Mottana, F. Seifert, Eur. J. Mineral. 14 (2002) 429-436.
[232] G. Artioli, S. Quartieri, A. Deriu, Can. Mineral. 33 (1995) 67-75.
[233] G. Cruciani, P.F. Zanazzi, S. Quartieri, Eur. J. Mineral. 7 (1995) 255-265.
[234] E. Borfecchia, L. Mino, D. Gianolio, C. Groppo, N. Malaspina, G. Martinez-Criado, J.A. Sans, S. Poli, D. Castelli, C. Lamberti, J. Anal. At. Spectrom. 27 (2012) 1725-1733.
[235] L. Mino, E. Borfecchia, C. Groppo, D. Castelli, G. Martinez-Criado, R. Spiess, C. Lamberti, Catal. Today. 229 (2014) 72-79.
[236] Z.Y. Wu, C.R. Natoli, A. Marcelli, E. Paris, F. Seifert, J. Zhang, T. Liu, J. Synchrot. Radiat. 8 (2001) 215-217.
[237] Z.Y. Wu, E. Paris, G. Giuli, A. Mottana, F. Seifert, J. Synchrot. Radiat. 8 (2001) 966-968.
[238] Z.Y. Wu, D.C. Xian, C.R. Natoli, A. Marcelli, E. Paris, A. Mottana, Appl. Phys. Lett. 79 (2001) 1918-1920.

[239] Z.Y. Wu, A. Mottana, A. Marcelli, E. Paris, G. Giuli, G. Cibin, Phys. Rev. B. 69 (2004) Art. n. 104106.
[240] G.J. Long, A.K. Cheetham, P.D. Battle, Inorg. Chem. 22 (1983) 3012-3016.
[241] E.M. El-Malki, R.A. van Santen, W.M.H. Sachtler, J. Catal. 196 (2000) 212-223.
[242] P. Fejes, K. Lazar, I. Marsi, A. Rockenbauer, L. Korecz, J.B. Nagy, S. Perathoner, G. Centi, Appl. Catal. A-Gen. 252 (2003) 75-90.
[243] L.V. Pirutko, V.S. Chernyavsky, A.K. Uriarte, G.I. Panov, Appl. Catal. A-Gen. 227 (2002) 143-157.
[244] E.J.M. Hensen, Q. Zhu, M.M.M. Hendrix, A.R. Overweg, P.J. Kooyman, M.V. Sychev, R.A. van Santen, J. Catal. 221 (2004) 560-574.
[245] E.J.M. Hensen, Q. Zhu, R.A. van Santen, J. Catal. 220 (2003) 260-264.
[246] B. Wichterlova, Z. Sobalik, J. Dedecek, Appl. Catal. B-Environ. 41 (2003) 97-114.
[247] G. Dalba, P. Fornasini, F. Rocca, Phys. Rev. B. 47 (1993) 8502-8514.
[248] S.A. Beccara, G. Dalba, P. Fornasini, R. Grisenti, A. Sanson, Phys. Rev. Lett. 89 (2002) Art. No. 025503.
[249] E. Bus, J.T. Miller, A. Jeremy Kropf, R. Prins, J.A. van Bokhoven, Physical Chemistry Chemical Physics. 8 (2006) 3248-3258.
[250] A. Bhan, W.N. Delgass, Catal. Rev.-Sci. Eng. 50 (2008) 19-151.
[251] J.M. Thomas, X. Liu, J. Phys. Chem. 90 (1986) 4843-4847.
[252] H. Kitagawa, Y. Sendoda, Y. Ono, J. Catal. 101 (1986) 12-18.
[253] A.Y. Khodakov, L.M. Kustov, T.N. Bondarenko, A.A. Dergachev, V.B. Kazansky, K.M. Minachev, G. Borbely, H.K. Beyer, Zeolites. 10 (1990) 603-607.
[254] N. Katada, S. Kuroda, M. Niwa, Appl. Catal. A-Gen. 180 (1999) L1-L3.
[255] P. Meriaudeau, C. Naccache, J. Mol. Catal. 59 (1990) L31-L36.
[256] Y. Ono, K. Kanae, J. Chem. Soc.-Faraday Trans. 87 (1991) 669-675.
[257] C.R. Bayense, A. Vanderpol, J.H.C. Vanhooff, Appl. Catal. 72 (1991) 81-98.
[258] B.S. Kwak, W.M.H. Sachtler, J. Catal. 145 (1994) 456-463.
[259] O. Otero Areán, G. Turnes Palomino, F. Geobaldo, A. Zecchina, J. Phys. Chem. 100 (1996) 6678-6690.
[260] C.R. Bayense, J.H.C. Vanhooff, A.P.M. Kentgens, J.W. Dehaan, L.J.M. Vandeven, J. Chem. Soc. Chem. Commun. (1989) 1292-1293.
[261] S.A. Axon, K. Huddersman, J. Klinowski, Chem. Phys. Lett. 172 (1990) 398-404.
[262] P. Behrens, H. Kosslick, V.A. Tuan, M. Froba, F. Neissendorfer, Microporous Mater. 3 (1995) 433-441.
[263] C. Lamberti, G.T. Palomino, S. Bordiga, A. Zecchina, G. Spano, C.O. Arean, Catal. Lett. 63 (1999) 213-216.
[264] C. Prieto, T. Blasco, M. Camblor, J. Perez-Pariente, J. Mater. Chem. 10 (2000) 1383-1387.
[265] S.H. Kim, J. Lee, S.J. Cho, C.H. Shin, N.H. Heo, S.B. Hong, Microporous Mesoporous Mat. 114 (2008) 343-351.
[266] K.A. Al-majnouni, N.D. Hould, W.W. Lonergan, D.G. Vlachos, R.F. Lobo, J. Phys. Chem. C. 114 (2010) 19395-19405.
[267] G.D. Meitzner, E. Iglesia, J.E. Baumgartner, E.S. Huang, J. Catal. 140 (1993) 209-225.
[268] E.J.M. Hensen, M. Garcia-Sanchez, N. Rane, P. Magusin, P.H. Liu, K.J. Chao, R.A. van Santen, Catal. Lett. 101 (2005) 79-85.
[269] A.C. Faro, V.D. Rodrigues, J.G. Eon, J. Phys. Chem. C. 115 (2011) 4749-4756.
[270] K. Okumura, K. Nishigaki, M. Niwa, Microporous Mesoporous Mat. 44 (2001) 509-516.
[271] R.I. Walton, D. O'Hare, J. Phys. Chem. Solids. 62 (2001) 1469-1479.
[272] L. Regli, S. Bordiga, C. Lamberti, K.P. Lillerud, S.I. Zones, A. Zecchina, J. Phys. Chem. C. 111 (2007) 2992-2999.
[273] L. Regli, C. Lamberti, C. Busco, A. Zecchina, C. Prestipino, K.P. Lillerud, S.I. Zones, S. Bordiga, Stud. Surf. Sci. Catal. 170 (2007) 585-593.

[274] L. Regli, S. Bordiga, C. Busco, C. Prestipino, P. Ugliengo, A. Zecchina, C. Lamberti, J. Am. Chem. Soc. 129 (2007) 12131-12140.
[275] H.B. Liu, G.Q. Shen, X.Q. Wang, J.Z. Wei, D.Z. Shen, Prog. Cryst. Growth Charact. Mater. 40 (2000) 235-241.
[276] K. Blaszczak, A. Adamczyk, M. Wedzikowska, M. Rokita, J. Mol. Struct. 704 (2004) 275-279.
[277] O.M. Moon, B.C. Kang, S.B. Lee, J.H. Boo, Thin Solid Films. 464 (2004) 164-169.
[278] M.E. Fleet, S. Muthupari, Am. Miner. 85 (2000) 1009-1021.
[279] T. Hemraj-Benny, S. Banerjee, S. Sambasivan, D.A. Fischer, W. Han, J.A. Misewichd, S.S. Wong, Physical Chemistry Chemical Physics. 7 (2005) 1103-1106.
[280] R. Carboni, G. Pacchioni, M. Fanciulli, A. Giglia, N. Mahne, M. Pedio, S. Nannarone, F. Boscherini, Appl. Phys. Lett. 83 (2003) 4312-4314.
[281] J. Stöhr, NEXAFS spectroscopy, Springer-Verlag, Berlin, 1992.
[282] T. Chapus, A. Tuel, Y.B. Taarit, C. Naccache, Zeolites. 14 (1994) 349-355.
[283] Y.J. Wang, X.H. Tang, R.Z. Zhu, L.R. Pan, Chem. J. Chin. Univ.-Chin. 21 (2000) 999-1004.
[284] N.N. Tusar, N.Z. Logar, I. Arcon, F. Thibault-Starzyk, A. Ristic, N. Rajic, V. Kaucic, Chem. Mat. 15 (2003) 4745-4750.
[285] C. Perego, A. Carati, P. Ingallina, M.A. Mantegazza, G. Bellussi, Appl. Catal. A-Gen. 221 (2001) 63-72.
[286] P. Wu, Y. Kubota, T. Yokoi, ACS Catal. 4 (2014) 23-30.
[287] D.C.M. Dutoit, M. Schneider, A. Baiker, J. Catal. 153 (1995) 165-176.
[288] E. Jorda, A. Tuel, R. Teissier, J. Kervennal, J. Catal. 175 (1998) 93-107.
[289] T. Maschmeyer, F. Rey, G. Sankar, J.M. Thomas, Nature. 378 (1995) 159-162.
[290] S. Krijnen, B.L. Mojet, H.C.L. Abbenhuis, J.H.C. Van Hooff, R.A. Van Santen, Physical Chemistry Chemical Physics. 1 (1999) 361-365.
[291] M.D. Alba, Z.H. Luan, J. Klinowski, J. Phys. Chem. 100 (1996) 2178-2182.
[292] J.M. Thomas, G. Sankar, Accounts Chem. Res. 34 (2001) 571-581.
[293] A. Corma, V. Fornes, S.B. Pergher, T.L.M. Maesen, J.G. Buglass, Nature. 396 (1998) 353-356.
[294] F.X. Gao, T. Yamase, H. Suzuki, J. Mol. Catal. A. 180 (2002) 97-108.
[295] O.A. Kholdeeva, T.A. Trubitsina, R.I. Maksimovskaya, A.V. Golovin, W.A. Neiwert, B.A. Kolesov, X. López, J.M. Poblet, Inorg. Chem. 43 (2004) 2284-2292.
[296] M. Taramasso, G. Perego, B. Notari, 1983.
[297] T. Blasco, M. Camblor, A. Corma, J. Pérez-Parriente, J. Am. Chem. Soc. 115 (1993) 11806-11813.
[298] G.N. Vayssilov, Catal. Rev.-Sci. Eng. 39 (1997) 209-251.
[299] P. Ratnasamy, D. Srinivas, H. Knözinger, Adv. Catal. 48 (2004) 1-169.
[300] S. Bordiga, A. Damin, F. Bonino, C. Lamberti, in: C. Copéret, B. Chaudret (Eds.), Surface and Interfacial Organometallic Chemistry and Catalysis, Springer-Verlag GmbH, Heidelberg, 2005, pp. 37-68.
[301] S. Bordiga, F. Bonino, A. Damin, C. Lamberti, Physical Chemistry Chemical Physics. 9 (2007) 4854-4878.
[302] C. Lamberti, S. Bordiga, A. Zecchina, A. Carati, A.N. Fitch, G. Artioli, G. Petrini, M. Salvalaggio, G.L. Marra, J. Catal. 183 (1999) 222-231.
[303] C. Lamberti, S. Bordiga, A. Zecchina, G. Artioli, G.L. Marra, G. Spanò, J. Am. Chem. Soc. 123 (2001) 2204-2212.
[304] R. Millini, E.P. Massara, G. Perego, G. Bellussi, J. Catal. 137 (1992) 497-503.
[305] R. Millini, G. Perego, D. Berti, W.O. Parker, A. Carati, G. Bellussi, Microporous Mesoporous Mater. 35-36 (2000) 387-403.
[306] M.R. Boccuti, K.M. Rao, A. Zecchina, L. G., G. Petrini, Stud. Surf. Sci. Catal. 48 (1989) 133.
[307] D. Scarano, A. Zecchina, S. Bordiga, F. Geobaldo, G. Spoto, G. Petrini, G. Leofanti, M. Padovan, G. Tozzola, J. Chem. Soc. Faraday Trans. 89 (1993) 4123-4130.

[308] S. Bordiga, F. Boscherini, S. Coluccia, F. Genoni, C. Lamberti, G. Leofanti, L. Marchese, G. Petrini, G. Vlaic, A. Zecchina, Catal. Lett. 26 (1994) 195-208.
[309] S. Bordiga, S. Coluccia, C. Lamberti, L. Marchese, A. Zecchina, F. Boscherini, F. Buffa, F. Genoni, G. Leofanti, G. Petrini, G. Vlaic, J. Phys. Chem. 98 (1994) 4125-4132.
[310] S. Bordiga, A. Damin, F. Bonino, A. Zecchina, G. Spanò, F. Rivetti, V. Bolis, C. Lamberti, J. Phys. Chem. B. 106 (2002) 9892-9905.
[311] G. Ricchiardi, A. Damin, S. Bordiga, C. Lamberti, G. Spanò, F. Rivetti, A. Zecchina, J. Am. Chem. Soc. 123 (2001) 11409-11419.
[312] S. Bordiga, A. Damin, F. Bonino, Z. A., C. Lamberti, Prepr. Pap.-Am. Chem. Soc., Div. Pet. Chem. 52 (2007) 196-200.
[313] A. Damin, G. Ricchiardi, S. Bordiga, A. Zecchina, F. Ricci, G. Spano, C. Lamberti, Stud. Surf. Sci. Catal. 140 (2001) 195-208.
[314] A. Damin, S. Bordiga, A. Zecchina, C. Lamberti, J. Chem. Phys. 117 (2002) 226-237.
[315] A. Damin, F. Bonino, G. Ricchiardi, S. Bordiga, A. Zecchina, C. Lamberti, J. Phys. Chem. B. 106 (2002) 7524-7526.
[316] A. Damin, S. Bordiga, A. Zecchina, K. Doll, C. Lamberti, J. Chem. Phys. 118 (2003) 10183-10194.
[317] A. Damin, F.X. Llabrés i Xamena, C. Lamberti, B. Civalleri, C.M. Zicovich-Wilson, A. Zecchina, J. Phys. Chem. B. 108 (2004) 1328-1336.
[318] L. Bonoldi, C. Busetto, A. Congiu, G. Marra, G. Ranghino, M. Salvataggio, G. Spanò, E. Giamello, Spectrochim. Acta A. 58 (2002) 1143-1154.
[319] S. Bordiga, G.T. Palomino, A. Zecchina, G. Ranghino, E. Giamello, C. Lamberti, J. Chem. Phys. 112 (2000) 3859-3867.
[320] F. Bonino, A. Damin, G. Ricchiardi, Ricci M, Spanò G, D'Aloisio R, Zecchina A, Lamberti C, Prestipino C, S. Bordiga, J. Phys. Chem. B. 108 (2004) 3573-3583.
[321] C. Prestipino, F. Bonino, A. Usseglio Nanot, A. Damin, A. Tasso, M.G. Clerici, S. Bordiga, F. D'Acapito, A. Zecchina, C. Lamberti, ChemPhysChem. 5 (2004) 1799-1804.
[322] T. Blasco, A. Corma, M.T. Navarro, J.P. Pariente, J. Catal. 156 (1995) 65-74.
[323] T. Blasco, M.A. Camblor, A. Corma, P. Esteve, J.M. Guil, A. Martinez, J.A. Perdigon-Melon, S. Valencia, J. Phys. Chem. B. 102 (1998) 75-88.
[324] M.A. Camblor, A. Corma, J. Perezpariente, Zeolites. 13 (1993) 82-87.
[325] P.E. Sinclair, G. Sankar, C.R.A. Catlow, J.M. Thomas, T. Maschmeyer, J. Phys. Chem. B. 101 (1997) 4232-4237.
[326] G. Sankar, J.M. Thomas, C.R.A. Catlow, C.M. Barker, D. Gleeson, N. Kaltsoyannis, J. Phys. Chem. B. 105 (2001) 9028-9030.
[327] M. Mazaj, W.J.J. Stevens, N.Z. Logar, A. Ristic, N.N. Tusar, I. Arcon, N. Daneu, V. Meynen, P. Cool, E.F. Vansant, V. Kaucic, Microporous Mesoporous Mat. 117 (2009) 458-465.
[328] S. Yuan, L. Shi, K. Mori, H. Yamashita, Mater. Lett. 62 (2008) 3028-3030.
[329] E.A. Eilertsen, F. Giordanino, C. Lamberti, S. Bordiga, A. Damin, F. Bonino, U. Olsbye, K.P. Lillerud, Chem. Commun. 47 (2011) 11867-11869.
[330] E.A. Eilertsen, S. Bordiga, C. Lamberti, A. Damin, F. Bonino, B. Arstad, S. Svelle, U. Olsbye, K.P. Lillerud, ChemCatChem. 3 (2011) 1869-1871.
[331] V. Bolis, S. Bordiga, C. Lamberti, A. Zecchina, A. Carati, F. Rivetti, G. Spano, G. Petrini, Microporous Mesoporous Mater. 30 (1999) 67-76.
[332] V. Bolis, S. Maggiorini, L. Meda, F. D'Acapito, G.T. Palomino, S. Bordiga, C. Lamberti, J. Chem. Phys. 113 (2000) 9248-9261.
[333] G. Ricchiardi, A. de Man, J. Sauer, Physical Chemistry Chemical Physics. 2 (2000) 2195-2204.
[334] A.J.M. de Man, J. Sauer, J. Phys. Chem. 100 (1996) 5025-5034.
[335] C.M. Zicovich-Wilson, R. Dovesi, J. Phys. Chem. B. 102 (1998) 1411-1417.
[336] C.M. Zicovich-Wilson, R. Dovesi, A. Corma, J. Phys. Chem. B. 103 (1999) 988-994.

[337] E. Fois, A. Gamba, E. Spano, J. Phys. Chem. B. 108 (2004) 9557-9560.
[338] E. Fois, A. Gamba, E. Spano, J. Phys. Chem. B. 108 (2004) 154-159.
[339] E. Fois, A. Gamba, G. Tabacchi, ChemPhysChem. 6 (2005) 1237-1239.
[340] A. Gamba, G. Tabacchi, E. Fois, J. Phys. Chem. A. 113 (2009) 15006-15015.
[341] E. Gallo, C. Lamberti, P. Glatzel, Physical Chemistry Chemical Physics. 13 (2011) 19409-19419.
[342] E. Gallo, F. Bonino, J.C. Swarbrick, T. Petrenko, A. Piovano, S. Bordiga, D. Gianolio, E. Groppo, F. Neese, C. Lamberti, P. Glatzel, ChemPhysChem. 14 (2013) 79-83.
[343] G.N. Vayssilov, R.A. van Santen, J. Catal. 175 (1998) 170-174.
[344] E. Paris, A. Mottana, G. Dellaventura, J.L. Robert, Eur. J. Mineral. 5 (1993) 455-464.
[345] F. Farges, G.E. Brown, J.J. Rehr, Geochim. Cosmochim. Acta. 60 (1996) 3023-3038.
[346] F. Farges, G.E. Brown, J.J. Rehr, Phys. Rev. B. 56 (1997) 1809-1819.
[347] S. Quartieri, G. Antonioli, G. Artioli, P.P. Lottici, Eur. J. Mineral. 5 (1993) 1101-1109.
[348] R.J. Davis, Z. Liu, J.E. Tabora, W.S. Wieland, Catal. Lett. 34 (1995) 101-113.
[349] C. Lamberti, S. Bordiga, D. Arduino, A. Zecchina, F. Geobaldo, G. Spanò, F. Genoni, G. Petrini, A. Carati, F. Villain, G.J. Vlaic, J. Phys. Chem. B. 102 (1998) 6382-6390.
[350] D. Gleeson, G. Sankar, C.R.A. Catlow, J.M. Thomas, G. Spanó, S. Bordiga, A. Zecchina, C. Lamberti, Physical Chemistry Chemical Physics. 2 (2000) 4812-4817.
[351] Z.Y. Wu, G. Ouvrard, P. Gressier, C.R. Natoli, Phys. Rev. B. 55 (1997) 10382-10391.
[352] D. Cabaret, Y. Joly, H. Renevier, C.R. Natoli, J. Synchrot. Radiat. 6 (1999) 258-260.
[353] G. Sankar, R.G. Bell, J.M. Thomas, M.W. Anderson, P.A. Wright, J. Rocha, J. Phys. Chem. 100 (1996) 449-452.
[354] C. Prestipino, P.L. Solari, C. Lamberti, J. Phys. Chem. B. 109 (2005) 13132-13137.
[355] P. Glatzel, U. Bergmann, Coord. Chem. Rev. 249 (2005) 65-95.
[356] J. Singh, C. Lamberti, J.A. van Bokhoven, Chem. Soc. Rev. 39 (2010) 4754-4766.
[357] M.H. Tuilier, A. Lopez, J.L. Guth, H. Kessler, Zeolites. 11 (1991) 662-665.
[358] A. Ghosh, N.G. Vargas, S.F. Mitchell, S. Stevenson, D.F. Shantz, J. Phys. Chem. C. 113 (2009) 12252-12259.
[359] S.R. Bare, S.D. Kelly, W. Sinkler, J.J. Low, F.S. Modica, S. Valencia, A. Corma, L.T. Nemeth, J. Am. Chem. Soc. 127 (2005) 12924-12932.
[360] L. Nemeth, J. Moscoso, N. Erdman, S.R. Bare, A. Oroskar, S.D. Kelly, A. Corma, S. Valencia, M. Renz, Stud. Surf.e Sci. Catal. 154 (2004) 2626-2631.
[361] P. Maki-Arvela, N. Kumar, S.F. Diaz, A. Aho, M. Tenho, J. Salonen, A.R. Leino, K. Kordas, P. Laukkanen, J. Dahl, I. Sinev, T. Salmi, D.Y. Murzin, J. Mol. Catal. A-Chem. 366 (2013) 228-237.
[362] D.H. Olson, N. Khosrovani, A.W. Peters, B.H. Toby, J. Phys. Chem. B. 104 (2000) 4844-4848.
[363] M. Milanesio, C. Lamberti, R. Aiello, F. Testa, M. Piana, D. Viterbo, J. Phys. Chem. B. 104 (2000) 9951-9953.
[364] M. Milanesio, D. Viterbo, L. Palin, G.L. Marra, C. Lamberti, R. Aiello, F. Testa, Stud. Surf. Sci. Catal. 142 (2002) 1891-1898.
[365] L. Palin, C. Lamberti, A. Kvick, F. Testa, R. Aiello, M. Milanesio, D. Viterbo, J. Phys. Chem. B. 107 (2003) 4034-4042.
[366] J.A. van Bokhoven, T.L. Lee, M. Drakopoulos, C. Lamberti, S. Thiess, J. Zegenhagen, Nat. Mater. 7 (2008) 551-555.
[367] K.K. Shah, J. Saikia, D. Saikia, A.K. Talukdar, Mater. Chem. Phys. 134 (2012) 43-49.
[368] D.S. Bhange, V. Ramaswamy, Mater. Res. Bull. 42 (2007) 851-860.
[369] A. Bhaumik, S.G. Hegde, R. Kumar, Catal. Lett. 35 (1995) 327-334.
[370] H.D. Pastore, Quim. Nova. 19 (1996) 372-376.
[371] S.L. Suib, Annu. Rev. Mater. Sci. 26 (1996) 135-151.
[372] M.A. Banares, Catal. Today. 51 (1999) 319-348.
[373] S. Dzwigaj, Curr. Opin. Solid State Mat. Sci. 7 (2003) 461-470.

[374] M. Anpo, S. Dzwigaj, M. Che, Adv. Catal. 52 (2009) 1-42.
[375] I.E. Wachs, C.A. Roberts, Chem. Soc. Rev. 39 (2010) 5002-5017.
[376] M. Anpo, S.G. Zhang, H. Yamashita, Stud. Surf. Sci. Catal. 101 (1996) 941-950.
[377] M. Anpo, S.G. Zhang, H. Mishima, M. Matsuoka, H. Yamashita, Catal. Today. 39 (1997) 159-168.
[378] M. Anpo, S.G. Zhang, S. Higashimoto, M. Matsuoka, H. Yamashita, Y. Ichihashi, Y. Matsumura, Y. Souma, J. Phys. Chem. B. 103 (1999) 9295-9301.
[379] S. Higashimoto, M. Matsuoka, H. Yamashita, M. Anpo, Jpn. J. Appl. Phys. Part 1. 38 (1999) 47-50.
[380] D. Wei, H. Wang, X.B. Feng, W.T. Chueh, P. Ravikovitch, M. Lyubovsky, C. Li, T. Takeguchi, G.L. Haller, J. Phys. Chem. B. 103 (1999) 2113-2121.
[381] M. Matsuoka, S. Higashimoto, H. Yamashita, M. Anpo, Res. Chem. Intermed. 26 (2000) 85-92.
[382] K.J. Chao, A.C. Wei, J. Electron Spectrosc. Relat. Phenom. 119 (2001) 175-184.
[383] S. Higashimoto, M. Matsuoka, S.G. Zhang, H. Yamashita, O. Kitao, H. Hidaka, M. Anpo, Microporous Mesoporous Mat. 48 (2001) 329-335.
[384] S. Dzwigaj, M. Matsuoka, M. Anpo, M. Che, Res. Chem. Intermed. 29 (2003) 665-680.
[385] M. Anpo, M. Matsuoka, H. Mishima, H. Yamashita, Res. Chem. Intermed. 23 (1997) 197-217.
[386] S. Higashimoto, S.G. Zhang, H. Yamashita, Y. Matsumura, Y. Souma, M. Anpo, Chem. Lett. (1997) 1127-1128.
[387] M.A. Camblor, R.F. Lobo, H. Koller, M.E. Davis, Chem. Mat. 6 (1994) 2193-2199.
[388] A.K. Patra, A. Dutta, M. Pramanik, M. Nandi, H. Uyama, A. Bhaumik, ChemCatChem. 6 (2014) 220-229.
[389] C.I. Round, C.D. Williams, C.V.A. Duke, J. Therm. Anal. Calorim. 54 (1998) 901-911.
[390] X.H. Tang, J.Z. Wang, H.X. Li, Stud. Surf. Sci. Catal. 154 (2004) 782-787.
[391] S.J. Jong, S.F. Cheng, Appl. Catal. A-Gen. 126 (1995) 51-66.
[392] A. Lita, X.S. Ma, R.W. Meulenberg, T. van Buuren, A.E. Stiegman, Inorg. Chem. 47 (2008) 7302-7308.
[393] K.A. Lomachenko, C. Garino, E. Gallo, D. Gianolio, R. Gobetto, P. Glatzel, N. Smolentsev, G. Smolentsev, A.V. Soldatov, C. Lamberti, L. Salassa, Physical Chemistry Chemical Physics. 15 (2013) 16152-16159.
[394] K. Seenivasan, E. Gallo, A. Piovano, J.G. Vitillo, A. Sommazzi, S. Bordiga, C. Lamberti, P. Glatzel, E. Groppo, Dalton Trans. 42 (2013) 12706-12713.
[395] J.C. Swarbrick, Y. Kvashnin, K. Schulte, K. Seenivasan, C. Lamberti, P. Glatzel, Inorg. Chem. 49 (2010) 8323-8332.
[396] O.Y. Khyzhun, T. Strunskus, C. Woll, H. Gies, V. Staemmler, J. Chem. Phys. 129 (2008) 9.
[397] G.D. Pirngruber, J.D. Grunwaldt, P.K. Roy, J.A. van Bokhoven, O. Safonova, P. Glatzel, Catal. Today. 126 (2007) 127-134.
[398] E. Gallo, C. Lamberti, P. Glatzel, Inorg. Chem. 52 (2013) 5633-5635.
[399] L. Mino, V. Colombo, J.G. Vitillo, C. Lamberti, S. Bordiga, E. Gallo, P. Glatzel, A. Maspero, S. Galli, Dalton Trans. 41 (2012) 4012-4019.
[400] G.A. Waychunas, G.E. Brown, Jr., in: K.A. Hodgts, B. Hedman, J.E. Penner-Hahn (Eds.), EXAFS and Near Edge Structures III, Springer-Verlag, Berlin, 1984, pp. 336-342.
[401] R. Shannon, Acta Cryst. A. 32 (1976) 751-767.